IPPP/24/67
LTH-1385
FERMILAB-PUB-24-0748-T
ZU-TH 51/24
CERN-TH-2024-171
MCNET-24-17

Event generation with SHERPA 3

Enrico Bothmann[1], Lois Flower[2,3], Christian Gütschow[4,5], Stefan Höche[6], Mareen Hoppe[7], Joshua Isaacson[6], Max Knobbe[1,6], Frank Krauss[2], Peter Meinzinger[2,8], Davide Napoletano[9], Alan Price[10], Daniel Reichelt[2,11], Marek Schönherr[2], Steffen Schumann[1], and Frank Siegert[7]

[1] *Institut für Theoretische Physik, Georg-August-Universität Göttingen, Friedrich-Hund-Platz 1, 37077 Göttingen, Germany*
[2] *Institute for Particle Physics Phenomenology, Durham University, Durham DH1 3LE, UK*
[3] *Department of Mathematical Sciences, University of Liverpool, Liverpool L69 3BX, UK*
[4] *Department of Physics & Astronomy, University College London, Gower Street, WC1E 6BT, London, UK*
[5] *Centre for Advanced Research Computing, University College London, Gower Street, London, WC1E 6BT, UK*
[6] *Theoretical Physics Division, Fermi National Accelerator Laboratory, P.O. Box 500, Batavia, IL 60510, USA*
[7] *Institut für Kern- und Teilchenphysik, Technische Universität Dresden, 01062 Dresden, Germany*
[8] *Physik-Institut, Universität Zürich, Winterthurerstrasse 190, CH-8057 Zürich, Switzerland*
[9] *Università degli Studi di Milano-Bicocca & INFN, Piazza della Scienza 3, Milano 20126, Italy*
[10] *Jagiellonian University,ul. prof. Stanisława Łojasiewicza 11, 30-348 Kraków, Poland*
[11] *CERN, Theoretical Physics Department, CH-1211 Geneva 23, Switzerland*

Abstract: SHERPA is a general-purpose Monte Carlo event generator for the simulation of particle collisions in high-energy collider experiments. We summarise new developments, essential features, and ongoing improvements within the SHERPA 3 release series. Physics improvements include higher-order electroweak corrections, simulations of photoproduction and hard diffraction at NLO QCD, heavy-flavour matching in NLO multijet merging, spin-polarised cross section calculations, and a new model of colour reconnections. In addition, the modelling of hadronisation, the underlying event and QED effects in both production and decay has been improved, and the overall event generation efficiency has been enhanced.

Contents

1 Introduction

SHERPA is a multi-purpose Monte Carlo event generator for simulations in high-energy particle physics, mainly in the context of collider experiments. Event generators such as SHERPA play a unique role in the analysis of experimental data, the design, construction, and improvement of ongoing and future measurements, and the refinement and validation of theoretical ideas and their application to phenomenology [1,2]. The three large event generator projects HERWIG [3,4], PYTHIA [5,6] and SHERPA are central to the success of present and future collider experiments and contribute to the continued development of the field of particle physics, including in particular the analysis of data from recent and upcoming runs of the Large Hadron Collider (LHC). They are also crucial for the preparation of future experiments [7,8].

The current version of SHERPA builds on a series of previous developments [9–11], which successively broadened the range of physics effects that could be simulated with the generator. These effects span the full range of distance scales encountered in high-energy particle collisions, across multiple parts of a collision event. A general overview of the event structure typically found in LHC collisions is sketched in Fig. 1. The simulation of such events relies on the factorisation of perturbative QCD effects described by the hard

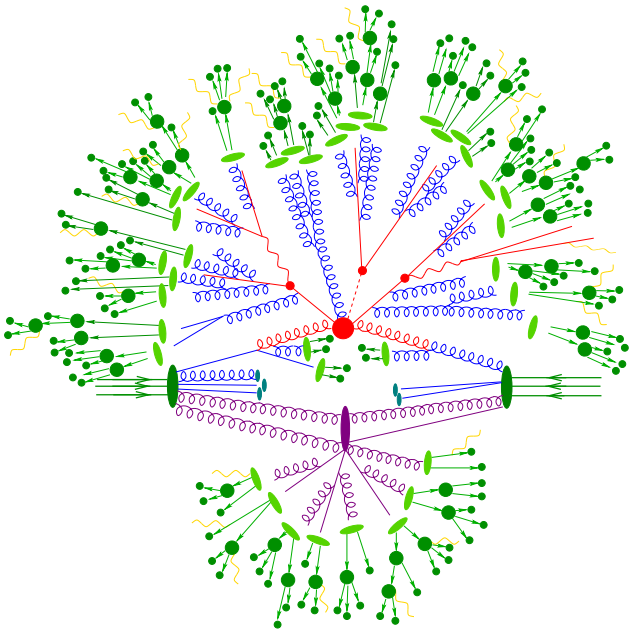

Figure 1: Event structure of a typical LHC collision. See the text for details.

collision (central red blob) from the QCD evolution (blue, tree-like structure), and the transition to the non-perturbative regime through the hadronisation process (light green blobs). Additional aspects are non-factorisable QCD corrections (purple blob and lines), the effects of QED and electroweak radiative corrections (yellow lines), and the decays of hadronic resonances (dark green blobs). The SHERPA framework is highly modular, in that the details of the physics models implementing these effects are separated from the interfaces that let different parts of the code interact with each other. This allows us to systematically improve or replace the implemented physics models, and to develop and add new models without deprecation of the old ones. The modular structure has proved particularly useful for the steady improvement of the formal perturbative accuracy achievable in SHERPA, for example the inclusion of higher-order electroweak corrections in different approximations, and the construction of new parton showers with increased logarithmic accuracy. Other recent examples include the addition of new models for non-perturbative physics, such as a dedicated module for the description of colour-reconnection effects.

In this manuscript we discuss some of these developments and recent additions in detail, focusing on the ones that significantly enhance the physics capabilities of SHERPA. They will be presented in Sec. 2 and include the following major new features:

- the computation of electroweak corrections at full NLO accuracy and in various approximations,
- higher-order QED corrections in production processes and from photon splittings in decays,

- spin-polarised cross section calculations,
- treatment of collider setups with resolved photons and other non-trivial beam spectra,
- heavy-flavour matching in multijet merging,
- improvements to the multiple interactions and hadronisation modelling,
- new models for beam remnants and colour reconnections, and
- technical developments leading to higher event generation efficiency.

In addition to its main use case for the simulation of exclusive final states at colliders, SHERPA also serves as a development platform for spin-off projects. For example, recent efforts enabled the support of automated or semi-automated resummation tools and event generation for neutrino physics within the SHERPA framework. In addition, we aim to address the physics simulation and computational needs of the LHC community and of future collider experiments not only by better physics modelling, but also by systematically enhancing the performance of the code through algorithmic improvements. These include AI/ML techniques, and developments for new hardware platforms, and will be described in Sec. 3.

All updates and new versions of SHERPA, including an extensive and up-to-date manual describing the technical details and options for running the code, are available online at

`https://sherpa-team.gitlab.io`.

The software download (see App. A) includes a pdf version of the relevant manual.

2 The physics model of the SHERPA Monte Carlo event generator

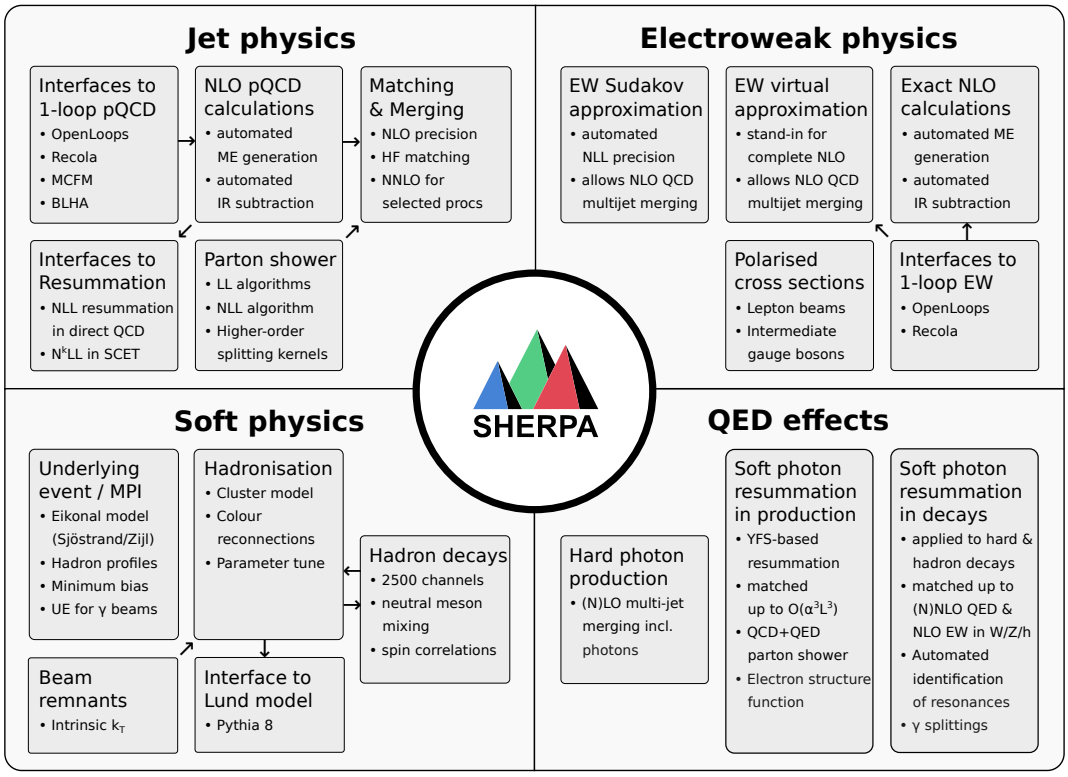

Figure 2: Schematic overview of the physics effects simulated by SHERPA, as well as major characteristics of their implementation in the event generator.

A schematic overview of the SHERPA 3 event generation framework is shown in Fig. 2. SHERPA itself is the centerpiece that coordinates the computation of QED, electroweak and QCD effects leading to the

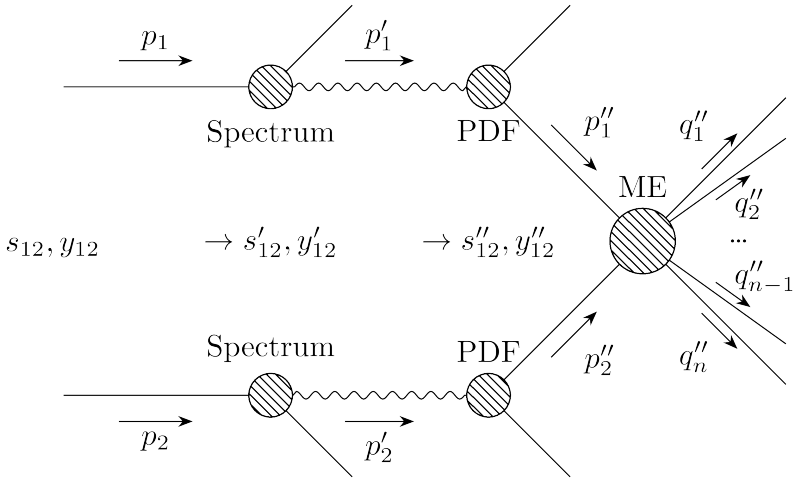

Figure 3: Incident-beam setup for SHERPA simulations. Each beam particle may (but does not have to) produce a secondary beam of particles parametrised by a beam spectrum. The secondary beam particles may (but do not have to) be resolved through a structure function or PDF. The emerging "partons" with momenta p_1'' and p_2'' then undergo a hard collision which is described by a matrix element (ME) and produces n final-state particles.

emergence of the many-body final state in a scattering experiment. We discuss these computations in detail in the following subsections thereby putting particular emphasis on newly added features in SHERPA 3.

2.1 The initial state

SHERPA is capable of simulating scattering events from a wide range of incident beam particles. This includes situations where an initial composite or elementary beam particle initiates a secondary beam particle according to a given momentum spectrum. The secondary beam particles themselves may be either composite or elementary. A prominent example is resolved vs. unresolved photons, where the former fluctuate into a hadronic structure with a parton distribution function (PDF) while the latter remain point-like. Accordingly, the sampling of the initial state comprises a two-stage procedure: The (optional) beam-spectrum sampling and the (optional) beam-substructure modelling through PDFs. Figure 3 illustrates the most general initial-state setup supported by SHERPA.

2.1.1 Beam spectra

Depending on the experimental situation, the particles which define the beam may produce other particles, and these secondary particles may produce the collision event instead. In these cases, the secondary beam particles follow a momentum distribution (a beam spectrum) which is either perturbatively calculable or can be parametrised. Such spectra are of prime importance to describe, for example, the interactions of photons from charged particle beams. SHERPA supports two methods to obtain photon beams: either via laser backscattering, where incident leptons convert to photons through Compton scattering, or via the Equivalent Photon Approximation (EPA). In the EPA the beam particles serve as quasi-classical sources of photons [12–14]. In SHERPA, the above spectra are implemented for electron/positron, (anti-)proton and ion beams. In the case of electrons, there are two versions, the original formula quoted in [14], and the improved version derived in [15]. Other available spectra are the pomeron and reggeon fluxes as used in parametrisations of Diffractive PDFs [16–18] to calculate diffractive jet production, see Sec. 2.4.2.

2.1.2 Parton densities and structure functions

To resolve the substructure of (composite) incoming particles, theoretical calculations make use of dedicated PDFs based on collinear factorisation. SHERPA provides access to all commonly used sets either through an

interface to LHAPDF [19], or through a dedicated interface which is specific to the required PDF.

For proton beams SHERPA defaults to the use of LHAPDF and the `PDF4LHC21_40_pdfas` PDF set [20]. See App. A for instructions on enabling LHAPDF support. If LHAPDF support is not enabled, dedicated interfaces to the NNPDF 3.1 PDF set [21] and the CT14 sets [22] are also provided. When using the LHAPDF interface, the value and the perturbative order for the running of α_s in SHERPA are automatically set to the values used in the PDF fit. At the expense of possible inconsistencies, the user can choose to override this behaviour by explicitly defining the value of $\alpha_s(m_Z^2)$ and the loop-order of its evolution. For the simulation of Multi-Parton Interactions (MPI, see Sec. 2.7), the PDFs can be selected independently. This treatment is motivated by the fact that the MPI tunes are highly sensitive to the PDFs and describe an effect beyond the collinear factorisation theorems underpinning the perturbative QCD calculations. While a different PDF potentially introduces small inconsistencies in the description of the parton content of a given proton, these mismatches lie entirely within the inherent uncertainties of the MPI model. It is recommended to use LHAPDF version 6.4.0 or later with SHERPA, as this version includes very significant performance improvements that are relevant for typical event generation use cases, benchmarked using standard SHERPA setups [23].

In case of incoming photons, either as a monochromatic beam or produced through one of the beam spectra described above, a range of PDF sets is supported, namely `GRV` [24,25], `GRS` [26], `SAL` [27], `CJK` [28,29], and `SaS` [30, 31], with the `SaS1M` set of the `SaS` family the default. For incident pomerons, which are only available as the product of a beam spectrum, the H1 Diffractive PDF fit has been interfaced [32]. Similary, for incident reggeons we default to the `GRVPI0` PDF fit in LHAPDF.

Finally, SHERPA provides an analytical QED structure function [33] for incoming lepton beams (electrons, positrons and (anti-)muons). It encodes the leading logarithmic (LL) corrections arising from collinear photon emissions, resummed using the DGLAP evolution equations. The resulting universal factors are matched to higher-order corrections, leading to some additional terms described in [34–37]. For details on the implementation see [38].

2.2 The hard scattering

The actual simulation of individual events starts from a partonic hard-scattering configuration, where the momenta of all initial and final state particles are distributed according to the corresponding transition matrix element. These matrix elements are stochastically sampled to determine the total inclusive production cross section as well as arbitrary differential distributions of final state particles. To address the large number of interesting scattering processes at the LHC and other past and future colliders, SHERPA's matrix element generators are built with a high degree of automation.

2.2.1 Hard scatterings at LO accuracy

SHERPA includes two in-house automated tree-level matrix element generators, AMEGIC [39] and COMIX [40]. They are capable of generating scattering matrix elements for any process within the Standard Model and a number of frequently used extensions like the Higgs Effective Field Theory (HEFT) [41–44], and are only limited by the available computing resources. Additionally, COMIX supports most models formulated using the UFO standard [45, 46], see Sec. 2.2.8.

When using either generator, it simultaneously generates suitable phase-space parametrisations using a combination of: inverse transform methods on propagator virtualities and polar angles [47], the multi-channel method described, e.g., in [48, 49], and VEGAS optimisation routines [50, 51]. Where appropriate, this also includes sampling of the colour and helicity spaces. This procedure allows for an efficient integration of multi-particle final states both in the bulk of the phase space and in intricate corners.

Finally, SHERPA also allows users to compute scattering cross sections for loop-induced processes, whose lowest-order contribution is mediated by one-loop diagrams. These calculations are facilitated by an interface to external one-loop providers, for details see Sec. 2.2.2. The phase-space parametrisations are obtained in a semi-automated fashion by using a tree-level proxy process which contains similar propagator and spin structures [52–55].

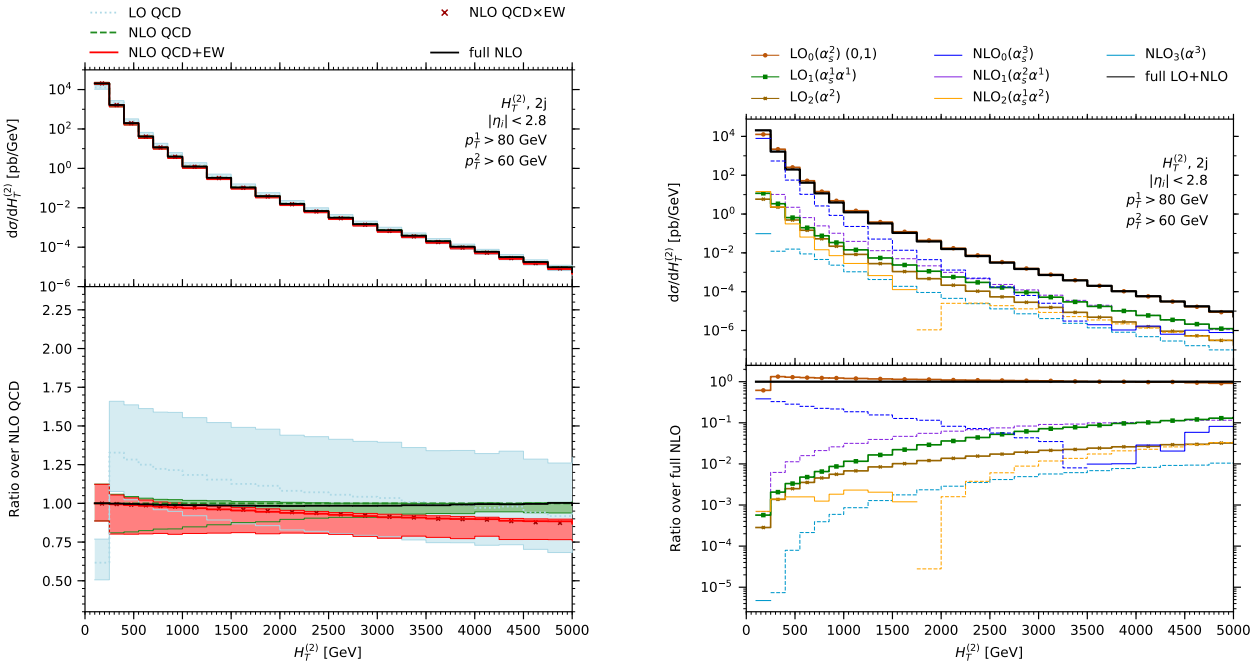

Figure 4: The full NLO corrections to the scalar sum of leading and sub-leading jet transverse momenta, $H_{\mathrm{T}}^{(2)}$ in inclusive dijet production at the LHC. The left panel shows the LO, NLO QCD, NLO QCD + EW, NLO QCD × EW, and full NLO results, including their scale uncertainties. The right panel shows the decomposition of the full NLO computation. The results were computed in the setup and the conventions of [64]. Dashed lines denote the absolute of an otherwise negative contribution.

2.2.2 Hard scatterings at NLO accuracy

Hard-scattering cross sections at NLO accuracy, comprising the inclusion of QCD, electroweak (EW), as well as mixed QCD-EW corrections, are computed by combining the Born-level expressions that constitute the LO expression and its real and virtual NLO corrections. When using a Monte Carlo integration framework, the calculation must be performed in four space-time dimensions, necessitating a subtraction formalism to render all integrands finite [56, 57]. In Sherpa, the Catani–Seymour subtraction formalism [57, 58] is used to construct the corresponding infrared subtraction terms. To assemble the tree-level expressions for Born and real-emission corrections, Sherpa relies on its matrix element generators Amegic and Comix, which also provide the corresponding phase-space parametrisations as described above. The infrared subtraction automatically identifies both QCD [59] and QED [60] divergences and constructs the relevant counterterms. Processes with simultaneous QCD and QED divergences can be handled by this procedure in Sherpa as well. External photons can be treated both as resolved and unresolved partons [60–64].

To compute the UV-renormalised one-loop corrections, Sherpa includes a small library of purpose-built renormalised one-loop matrix elements and provides a number of interfaces to one-loop providers (OLPs), namely OpenLoops [65, 66], Recola [67–69], or MadLoop [70]. A recent addition is the interface to MCFM [71]. MCFM's fast analytic one-loop matrix elements can provide significant overall event generation speed-ups, particularly when combined with Sherpa's pilot run strategy [23]. Details on how to enable Sherpa's OLP interfaces are given in App. A.

Figure 4 shows an example application of the above machinery to calculate the complete NLO predictions to inclusive dijet production at the LHC in the setup of [64]. This process, despite its limited number of external legs, is comprised of a multitude of subprocesses contributing at various different coupling orders in perturbation theory. As a consequence, the NLO corrections contain both QCD and QED divergences which must be addressed by a suitable subtraction procedure.

2.2.3 Hard scatterings at N^{2}LO accuracy

A few selected calculations of high phenomenological importance have been implemented in SHERPA at N^{2}LO precision. In particular, Drell–Yan lepton-pair production [72], Higgs-boson production [73] and Deep-Inelastic Scattering [74] simulations can be carried out fully differentially at the parton level, making use of q_T slicing [75, 76] or Projection-to-Born [77] techniques. The q_T slicing method separates the N^{2}LO corrections into a contribution with $q_T < q_{T,cut}$, the so-called zero-q_T bin, and the remaining spectrum with $q_T > q_{T,cut}$. The first contribution is integrated out analytically using approximate expressions that become exact in the limit $q_{T,cut} \to 0$. The second comprises an NLO calculation of the Born-plus-one-jet process and is computed using the tools introduced in the previous section. The Projection-to-Born method, on the other hand, introduces an arbitrary but infrared-safe and unambiguous mapping from the real and double-real phase spaces onto the Born phase space and evaluates all components of the N^{2}LO calculation using this mapping. Consequently, all singularities cancel locally in the Born phase space, leaving a finite result. The mismatch introduced by projecting the real and double-real phase-space contributions is corrected through dedicated lower-order calculations at NLO and LO, respectively, using the methods discussed in the previous sections.

2.2.4 Decays of unstable particles

Within SHERPA, there are various options to simulate the decays of massive unstable particles produced in the hard scattering process. A full off-shell treatment in the matrix element yields the most complete calculation, but might not always be feasible, either because of the inefficient generation of unweighted events due the high final-state complexity or because the user is interested in an inclusive simulation of multiple decay final states. For such cases, SHERPA provides a module to simulate decays in an automatic way [78].

In its automated treatment of massive unstable particle decays, SHERPA employs an improved narrow-width approximation, where the hard scattering of Secs. 2.2.1–2.2.3 constitutes the production process, while its decays are calculated at LO accuracy. Spin correlations are taken into account using the algorithm described in [79–82], and off-shell effects are modelled by *a posteriori* adjusting the resonance kinematics according to its Breit–Wigner distribution. QCD and QED radiative corrections can be effected through interfaces to SHERPA's parton shower and soft-photon resummation, see Secs. 2.3 and 2.6, respectively. Unless specified by the user, event-by-event decay channels are selected according to their branching ratios, determined from the automatically generated decay matrix elements and decay widths using tree-level expressions. Their generation is model-specific and, in addition to the Standard Model, is applicable to beyond the Standard Model theories using the UFO format (see Sec. 2.2.8 for details). This enables a decay simulation that is fully consistent with the production process.

The decay framework is used, for example, for Standard Model processes involving top quarks, massive vector bosons, or the Higgs boson. Decays can be added on top of a wide variety of simulations of the hard scattering, calculated both at LO and NLO, and both in fixed-order or in parton-shower matched/merged simulations.

2.2.5 Cross sections for polarised lepton beams

The ability to polarise the incoming beams is a defining feature of various proposed future lepton-collider experiments [83, 84]. Such setups can be used to considerably enhance signal rates while also suppressing unwanted background processes, because the cross sections of scattering processes within and beyond the Standard Model often depend on the helicities of incoming particles. By varying the polarisations of the incoming beams the properties of the produced final-state particles such as their chiral couplings and quantum numbers can be probed [85].

In SHERPA, it is possible to simulate events with longitudinally-polarised beams by reweighting the helicity amplitudes with the corresponding fractional polarisation, $P_{e^\pm}$, using the AMEGIC matrix element generator, which is a common approach in event generators [86, 87]. This can then be combined with a soft-photon resummation in the YFS formalism, as described in Sec. 2.6.4, to further improve the accuracy of the simulation. Since YFS resummation is based on the soft-photon limit, the matching of higher-order corrections with beam polarisation can be achieved in a straightforward fashion. This will allow SHERPA to provide NLO EW predictions for polarised collider experiments in the future. In Tab. 1 we illustrate the effect of beam polarisation on various relevant Higgs-boson production processes. It can be observed that

(P_{e^-}, P_{e^+})	HZ		$H\nu_e\bar{\nu}_e$		He^+e^-	
	$\sigma^{\mathrm{LO}}/\sigma^{\mathrm{LO}}_{(0,\,0)}$	$\sigma^{\mathrm{YFS}}/\sigma^{\mathrm{YFS}}_{(0,\,0)}$	$\sigma^{\mathrm{LO}}/\sigma^{\mathrm{LO}}_{(0,\,0)}$	$\sigma^{\mathrm{YFS}}/\sigma^{\mathrm{YFS}}_{(0,\,0)}$	$\sigma^{\mathrm{LO}}/\sigma^{\mathrm{LO}}_{(0,\,0)}$	$\sigma^{\mathrm{YFS}}/\sigma^{\mathrm{YFS}}_{(0,\,0)}$
(-0.8, 0)	1.17	1.17	1.70	1.68	1.18	1.19
(-0.8, 0.3)	1.47	1.47	2.20	2.18	1.49	1.50
(-0.8, -0.3)	0.87	0.87	1.20	1.19	0.87	0.88
(0.8, 0.0)	0.83	0.83	0.30	0.32	0.82	0.83
(0.8, 0.3)	0.65	0.65	0.32	0.34	0.65	0.65
(0.8, -0.3)	1.01	1.00	0.28	0.31	0.99	1.00

Table 1: Normalised cross sections for various $e^+e^- \to H + X$ production processes evaluated with different initial-state polarisation combinations at $\sqrt{s} = 380\,\mathrm{GeV}$, both at LO and including YFS corrections.

due to the chiral nature of the weak-current interaction significant enhancements or suppressions depending on the chosen initial-state polarisations can be realised. The YFS corrections included here are purely at the resummation level and are not matched to any higher-order corrections.

2.2.6 Cross sections for polarised intermediate gauge bosons

The ability to predict cross sections for polarised vector boson production is of great interest, as they probe the structure of the electroweak interaction. With Sherpa 3 it is now possible to compute cross sections for polarised intermediate vector bosons in the s-channel [88]. The efficiency of the implementation is guaranteed by the simultaneous computation of all polarisation combinations. Each combination is added as an additional event weight to the unpolarised sample, using the techniques described in [89]. The spin-correlated narrow-width approximation [78] is used to compute the various contributions (see Sec. 2.2.4 for details). The different polarisation components are based on the complete helicity-dependent amplitude, such that interferences between different polarisations are also accessible on an event-by-event basis. Within a single generator run, multiple reference frames can be studied.

The calculation of polarised cross sections is not limited to LO and can also be performed at approximate NLO QCD accuracy, referred to as nLO QCD. They can be matched to Sherpa's parton shower via the Mc@Nlo method and be included in multijet merging, see Sec. 2.4. Within the nLO QCD calculation, polarisation fractions are calculated depending on the event type in the Mc@Nlo formalism. For $\mathbb{H}$- and resolved $\mathbb{S}$-events, the corresponding amplitude information is constructed using the complete real emission corrections. Hence, the exact polarisation fractions, up to NLO QCD, are used for both soft and hard emissions. For unresolved $\mathbb{S}$-events, however, the amplitude information is based on the Born expression, i.e. all corrections stemming from virtual and ultra-soft and/or collinear emission are neglected. As the number of events in this category is generally exceedingly small in typical LHC setups, and in any case this construction is only used to determine the polarisation fractions in the otherwise fully NLO QCD-accurate unpolarised sample, the error introduced in this way is expected to be small.

Fig. 5 (left) shows the nLO QCD+PS contribution to polarised inclusive $\mathrm{W^+Z}$ production for the lepton rapidity in the laboratory frame, as an example. It illustrates the importance of including higher order QCD effects in polarisation templates, since they can be very large and non-trivial. Comparisons with complete NLO QCD fixed-order calculations [90] confirm that our nLO QCD approximation can reproduce all main contributions of the full calculation, as these are strongly dominated by real corrections. Hence, also multijet-merged calculations are able to describe the bulk of the NLO QCD effects, if small merging scales are used, as demonstrated on the right hand side of Fig. 5.

2.2.7 Physics within the Standard Model – instantons

In addition to standard perturbative scattering amplitudes, discussed in Secs. 2.2.1–2.2.3, the Standard Model contains other manifestly non-perturbative solutions like the QCD instanton [91], which emerge as a consequence of the non-trivial structure of the Yang–Mills vacuum [92,93]. While the QCD instanton violates B+L symmetries, it conserves B−L as well as chirality. Despite otherwise large inclusive production rates, the cross section falls rapidly with increasing instanton mass, and, as a consequence, the existence of instantons

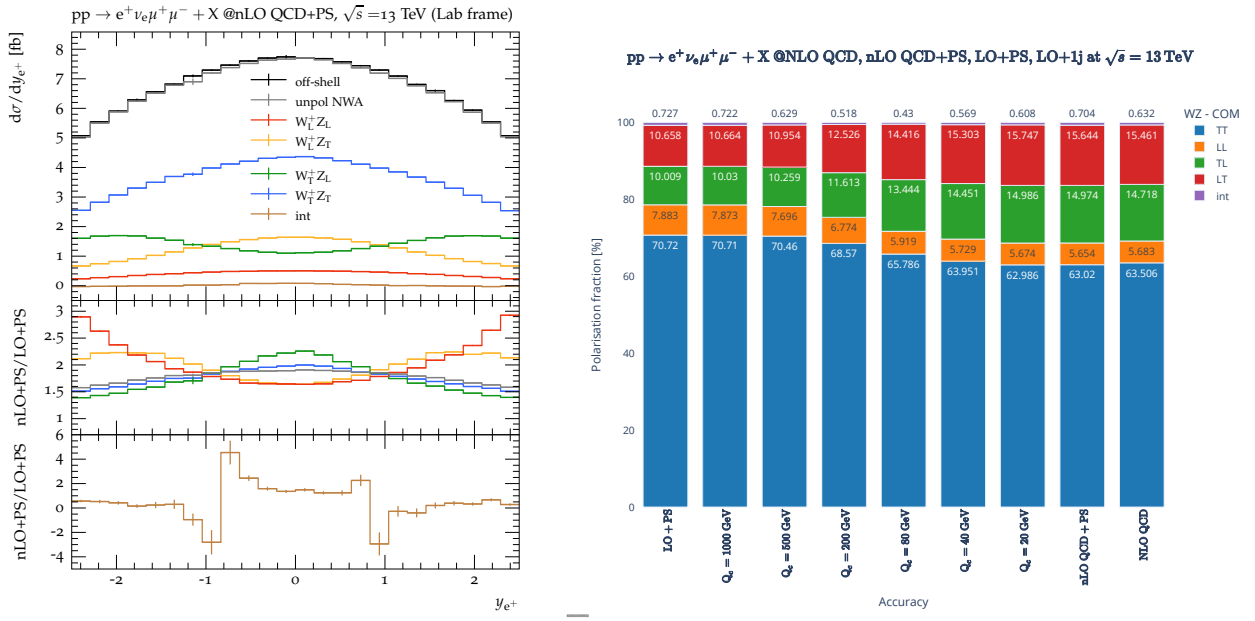

Figure 5: Left: Double-polarised distributions of the positron rapidity y_{e^+} in inclusive W^+Z production at nLO QCD+PS (polarised distribution)/ NLO QCD+PS (unpol, full) accuracy; polarisation states are defined in the laboratory (Lab). K-factors (bottom panel) are the ratio of n(N)LO QCD+PS over LO+PS cross sections. Right: Integrated polarisation fractions for inclusive W^+Z boson production at the LHC (13 TeV) for LO+1j simulations matched to parton shower using different merging scales. For comparison, also polarisation fractions at nLO QCD+PS and LO+PS, as well as at fixed NLO QCD taken from [90] are shown. The polarisation is defined in the W^+Z boson centre-of-mass frame. (Figures adapted from [88]).

has not been confirmed experimentally yet.

SHERPA comprises an implementation of QCD-instanton-mediated multiparton production processes [94], including important quantum corrections due to initial- and final-state gluon interactions. The $\hat{s}$-dependent production cross sections, where $\hat{s}$ is the partonic c.m. energy squared, is taken from an interpolation table included in the runcard. This table also provides results for different scale choices and allows, to some extent, to vary these scales to obtain some idea about related uncertainties. The outgoing quarks, anti-quarks, and a Poisson-distributed number of gluons populate the phase space isotropically in the instanton rest frame.

2.2.8 Physics models beyond the Standard Model – UFO

SHERPA provides a versatile framework for the simulation of new physics signals [78, 95], through built-in models (Higgs Effective Field Theory [41–44], the Minimal Supersymmetric Standard Model [96] with inputs in the SLHA format [97], and various anomalous Triple and Quartic Gauge Couplings Models [98–102]) or, more generally through a UFO [45] interface to COMIX. The latter has been used in a variety of analyses within the context of the Standard Model Effective Field Theory (SMEFT), see e.g. [103–105]. For details of how to enable SHERPA's UFO support during installation, see App. A.

Recently, the UFO format was updated to address and standardise several extensions that have been implemented since the first version was proposed [46], thus ensuring portability and compatibility between generators. The updated UFO opens new possibilities and options, such as customised propagators [106], the inclusion of particle decay information [107], and the renormalisation group running of model parameters [108], all of which are expected in future versions of SHERPA. In addition, it allows the inclusion of form factors associated with specific Lorentz structures in the vertices. These are enabled in SHERPA but currently need to be manually implemented; we expect this process to be semi-automatic in future releases.

2.3 Parton showers

The role of parton showers [109–112] and dipole showers [113–115] is to link the particles involved in the hard-scattering process, as well as in possible secondary scatterings, to an ensemble of comparably low-energetic QCD quanta that undergo hadronisation. SHERPA provides two built-in parton-shower algorithms, CSSHOWER and ALARIC. While the former is the current default, the latter is the development platform towards higher formal accuracy, including NLL and ultimately NLO QCD precision. In addition, the legacy algorithm DIRE is also still part of the code base.

2.3.1 LL accuracy – CSSHOWER and DIRE

SHERPA's default parton shower, called CSSHOWER [116], is based on Catani–Seymour dipole factorisation of NLO matrix elements for massless and massive partons [57, 58], as first suggested in [117]. CSSHOWER simulates emissions by splitting pseudo-dipoles involving an emitter and a spectator, each being either an initial or final-state particle, giving four types of dipole configuration. The shower evolution variable governing the sequence of emissions corresponds to the relative transverse momentum between emitter and emitted particle. For initial-state splittings, this is the transverse momentum with respect to the beam. Details on the available options for the momentum mapping and evolution variable are described in [118]. The CSSHOWER fully respects mass effects in the kinematics, allowing one to consistently perform four- and five-flavour scheme calculations [119, 120], see also Sec. 2.4.4. The CSSHOWER implementation provides all necessary functionalities and extensions for combining the shower with LO, NLO, and NNLO matrix elements, see Sec. 2.4. It also contains an implementation of QED splitting functions [121], which, when active, co-evolve with their QCD counterparts. A fully-fledged QED parton shower, which includes all dipoles, the full charge correlators and the correct collinear limit for photon splittings [60], will be included in a future release. The recommended option for including QED radiation in SHERPA, however, is the YFS soft-photon resummation, described in section 2.6.

The DIRE parton shower [122] is an alternative QCD evolution model within SHERPA, and served as a test bed for various systematic improvements. DIRE hosts the first implementation of fully exclusive triple-collinear and double-soft splitting functions, which are needed for any NLL accurate parton shower [123–125]. It has been shown [126] that the kinematic mappings in DIRE are not NLL safe, therefore the model has been deprecated and is no longer actively supported. We note, however, that a solution to the known NLL violation in DIRE at the level of the second emission was proposed in the context of the fully differential two-loop soft corrections [124]. This has inspired the development of the novel ALARIC parton-shower model, described in the following section.

2.3.2 NLL accuracy – ALARIC

In addition to SHERPA's default dipole-like parton shower described above, a new method for QCD evolution is implemented in the ALARIC module [127]*. It has been constructed to address the shortcomings of the CSSHOWER and DIRE wrt. their formal resummation accuracy pointed out in [126, 128] and has been shown to be NLL accurate [127]. The basic algorithm has since been extended to account for massive-quark effects [129], as well as multijet merging. Further studies have assessed the impact of certain uncertainties at sub-leading power that arise from different kinematics parametrisations [130]. A unique aspect of the ALARIC method is the non-trivial dependence of splitting functions on the azimuthal emission angle, even when spin correlations are not included. This allows simulation of the complete one-loop soft radiation pattern without the need for angular ordering. Since it is well known that kinematic edge effects play an important role in the effective description of data by parton showers [131], ALARIC allows the variation of key components such as the recoil system, evolution variable and splitting parameters in order to probe remaining ambiguities beyond NLL accuracy. ALARIC is the prospective default parton shower of future SHERPA releases, once crucial features including NLO matching and MEPS@NLO merging have been provided in full generality. The corresponding integrated splitting functions were presented for the massless and massive case in [127] and [129], respectively. In addition, ALARIC will be equipped with higher-order corrections to the splitting functions in a fully differential form, using the methods of [123–125].

We illustrate the quality of the predictions achieved by the ALARIC method in Fig. 6, where we compare

*Note that ALARIC is included as of release SHERPA-3.1.

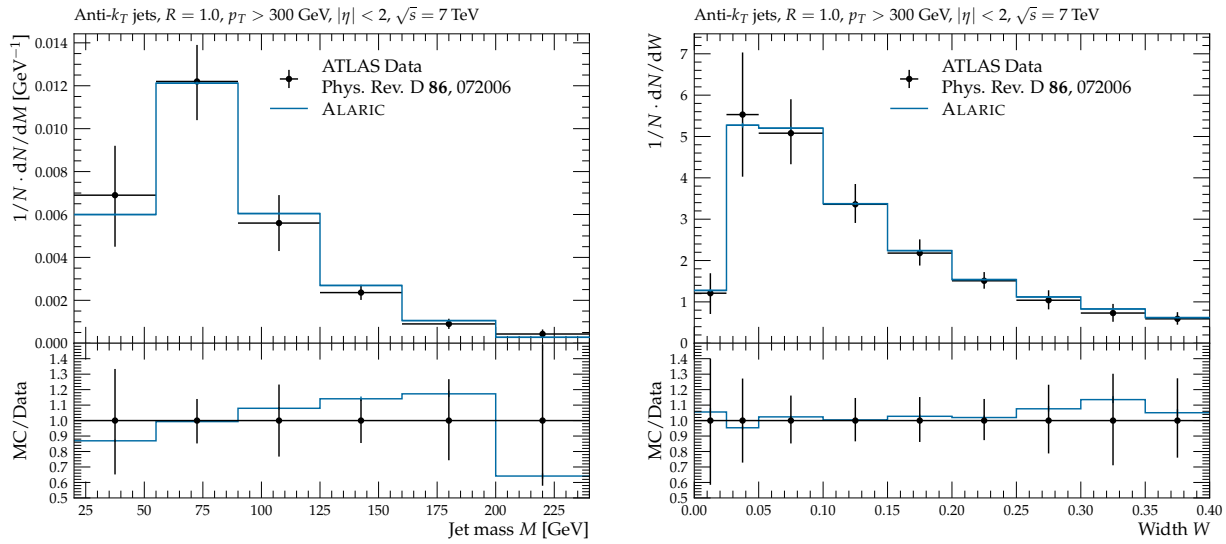

Figure 6: Jet mass and jet width measured by the ATLAS collaboration [132] at $\sqrt{s} = 7$ TeV, compared to predictions from ALARIC using the setup of [130].

to jet shape data measured by ATLAS at $\sqrt{s} = 7$ TeV [132]. We show the jet mass and jet width, measured on high transverse momentum jets $p_{\mathrm{T}} > 300$ GeV, clustered with the anti-k_t algorithm with $R = 1$, in the central rapidity region $|\eta| < 2$. We observe an excellent agreement, within the uncertainty of the experimental data. A more comprehensive overview of LHC phenomenology with ALARIC has been presented in [130].

2.4 Matching and multijet merging

Going beyond simulations at the lowest order in perturbation theory in an event generator, whether through the inclusion of either higher-order loop corrections or multiple-emission exact matrix elements, inevitably introduces overlap in the perturbative description of a scattering process between the hard matrix element and the parton-shower evolution. In this section we review the different options to address this problem.

2.4.1 NLO matching methods

To combine the higher-order calculations of Sec. 2.2.2 with the parton showers of Sec. 2.3, a number of techniques are available in the literature. While the most commonly used are known as MC@NLO [133] and POWHEG [134, 135], KRKNLO [136], UNLOPS [137], and the multiplicative-accumulative matching of [138] provide alternative formalisms. In SHERPA, the S-MC@NLO matching technique [139–141], an extension of the MC@NLO method, is used. The algorithm is implemented in complete generality, both for massless and for massive processes. It is the only publicly available implementation of a matching procedure that includes the complete colour and spin information of the matrix elements at the single-emission level for arbitrary hard processes. The matching has been compared against other, publicly available implementations of MC@NLO and POWHEG in a number of community studies, which found the expected level of agreement in the physics modelling between the various simulation tools [142, 143]. SHERPA's implementation of the matching procedure has also been tested in simulations of up to $W + 3$ jets [144] and $H + 3$ jets [145, 146] at NLO precision. Approximate NLO EW corrections can be included for almost every process, see Sec. 2.5.

In some carefully validated cases it can be beneficial to disable the full colour- and full spin-correlation treatments of the S-MC@NLO technique and fall back to the leading-colour spin-averaged approximations of the standard MC@NLO matching method. Combined with additional modifications that do not reduce the formal accuracy, this has been shown to reduce not only the negative weight fraction of inclusive event samples by a factor two [147], but also the average CPU resources required per unweighted event by a similar factor [23]. In a typical Z+jets or $t\bar{t}$+jets NLO multijet merged calculation, this translates into a significant reduction of the computing time required to further process the resulting event samples, e.g. for detector simulations.

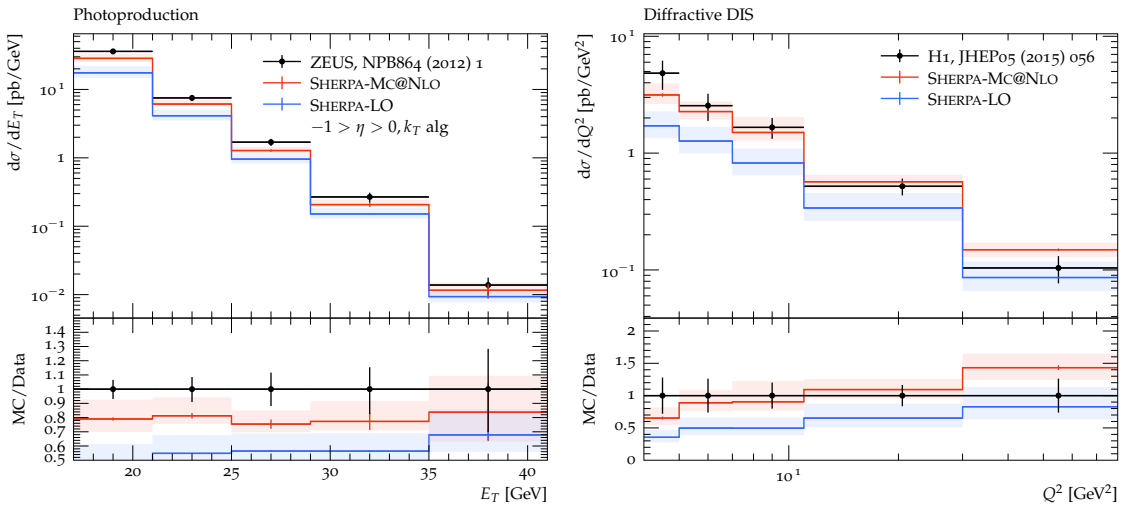

Figure 7: Left: Distribution of inclusive jet transverse energy for k_T-clustered jets in the pseudo-rapidity bin $-1 < \eta < 0$ in photoproduction, comparing SHERPA MC@NLO results with ZEUS Run 2 data [152]. Right: Distribution of photon virtuality Q^2 in diffractive DIS, comparing SHERPA leading order (LO) and MC@NLO results with H1 data [161].

For selected processes, SHERPA provides a matching of N^{2}LO matrix elements to its default shower using the UN^{2}LOPS method [137]. Such a matching is particularly useful to cross-check the quality of SHERPA's multijet merged simulations. Due to a large number of negative weights, however, we do not recommend the UN^{2}LOPS technique to be used directly in experimental simulation campaigns.

2.4.2 Photoproduction and hard diffraction at NLO

The NLO matching methods of the previous section have recently been applied to photoproduction and diffractive jet production. The photoproduction regime is characterised by beam-spectrum photons with a small virtuality, and gives significant contributions to the total cross section in lepton–lepton [148–150] and lepton–hadron [151–153] collisions, and has also been studied in ion–ion collisions in the context of Ultra Peripheral Collisions [154–157]. In contrast to regular NLO-matched calculations, photoproduction features a second convolution with a beam spectrum for the incident photons, see Sec. 2.1.1. In particular, while the flux of quasi-real photons is typically computed in the Equivalent Photon Approximation, these quasi-real photons are then resolved by means of parton-in-photon PDFs [30, 158]. These PDFs encode both non-perturbative contributions arising from the photons' mixing with neutral vector mesons (vector meson dominance), and perturbative contributions by means of $\gamma \to q\bar{q}$ splittings. Both these effects have to be combined with the "direct" interaction, where the photon remains intact. To match this computation at NLO, the varying beam energies as well as the QED and QCD divergences have to be taken into account. The latter can be handled by leveraging the combined automated QED+QCD subtraction, while for the former, the momentum fractions that appear in the matching algorithm must be computed with respect to the photon momentum given by the phase-space point. The implementation in SHERPA has been validated against data from LEP and HERA experiments [159]. An example is illustrated in the left plot in Fig. 7, where predictions at MC@NLO accuracy for jet production at HERA are compared to data from the ZEUS experiment [152]. We observe large corrections when comparing to LO, which can be associated with the phase space being filled up by the real correction. First matched NLO predictions for the EIC have been presented in [160].

Hard-diffractive events are defined by the beam proton undergoing an elastic scattering or dissociation into a low-mass excitation. Diffraction contributed about 10% to the total cross section at HERA [18], and will be studied at the EIC as well [162]. Diffractive jet production, including both diffractive DIS and diffractive photoproduction, has been implemented in SHERPA and validated against H1 and ZEUS data [163] by implementing an interface to the H1 DPDF fit and the corresponding flux [32]. The matching procedure is the same as for photoproduction, and we show a comparison to H1 data [161] for diffractive DIS in the right plot in Fig. 7. Again, large corrections can be seen with respect to LO, associated with filled-up

phase space. These methods have been used for predictions of diffraction at the EIC, and are the first fully-differential hadron-level calculations of hard diffraction at matched NLO accuracy [163]. Figure 7 shows a significant improvement compared to a leading-order prediction. Both the photoproduction and hard-diffraction implementations can also be applied at hadron colliders.

2.4.3 Multijet merging procedures

Process	Highest additional jet mult. at NLO	References	Comments
$e^+e^- \to$ hadrons	4	[164, 165]	
$e^+e^- \to e^+e^-jj$	–	[159]	in photoproduction limit
$ep \to e +$ jets	3	[74, 166]	in DIS limit
$ep \to ejj$	–	[159]	in photoproduction limit
$ep \to epjj$	–	[163]	diffractive photoproduction/DIS
$pp \to$ jets	3	[167]	
$pp \to V +$ jets	3	[144, 168]	
$pp \to \gamma +$ jets	2	[169]	
$pp \to H +$ jets	3	[118, 143, 145, 146]	ggF in HEFT, incl. finite m_t, m_b
$pp \to Vjj$	–	[170]	in VBF topologies
$pp \to Hjj$	–	[143]	in VBF topologies
$pp \to VV +$ jets	1	[52, 55, 171]	
$pp \to V\gamma +$ jets	1	[172]	
$pp \to \gamma\gamma +$ jet	1	[173, 174]	
$pp \to VH +$ jets	1	[53, 175, 176]	
$pp \to HH$	–	[54]	full loop-induced, incl. finite m_t
$pp \to VVjj$	–	[177]	t- (VBS), s-ch. (semilep. VVV)
$pp \to VVV +$ jets	1	[175]	
$pp \to VV\gamma$	–	[178]	
$pp \to V\gamma\gamma$	–	[179, 180]	
$pp \to \gamma\gamma\gamma +$ jets	1	[181]	
$pp \to \gamma\gamma\gamma\gamma$	–	[181]	
$pp \to tj$	–	[182]	t- and s-channel
$pp \to tW$	–	[182]	using diagram removal (DR)
$pp \to t\bar{t} +$ jets	2	[183, 184]	
$pp \to t\bar{t}V +$ jets	1	[185]	
$pp \to t\bar{t}\gamma +$ jets	1	[185]	
$pp \to t\bar{t}b\bar{b}$	–	[186]	full m_b dependence
$pp \to t\bar{t}t\bar{t}$	–	[185]	
$pp \to V +$ HF	2	[187]	in fusing scheme, see Sec. 2.4.4
$pp \to t\bar{t} +$ HF	2	[188]	in fusing scheme, see Sec. 2.4.4

Table 2: Usage of SHERPA's matching and merging capabilities in the literature. V generically denotes the off-shell production of a W or Z boson, decaying leptonically. Maximal jet multiplicities at NLO largely depend on the hardware available, the stated multiplicities correspond to the largest one that was used in the cited references and not a limitation in principle. In almost all cases additional multiplicities were merged on top of the quoted NLO multiplicities using the techniques of [168, 175, 189].

One of the strengths of the physics modelling with SHERPA is the control over both the matrix-element calculation and the parton-shower simulation in one single framework. This facilitates the implemention of techniques to systematically improve the simulation of jet production. Such methods include multijet merging at leading-order [190–194] and at next-to-leading order in QCD [137, 164, 168, 195–197]. SHERPA implements the leading-order merging methods described in [191,194], and the next-to-leading order techniques from [164, 168,175,189]. They incorporate leading-order or next-to-leading order calculations with sufficiently separated parton-level jets into parton-shower predictions, while maintaining both the logarithmic accuracy of the

parton shower resummation and the fixed-order accuracy of the hard matrix elements.

SHERPA's implementation of the matching and merging procedures at S-MC@NLO and MEPS@NLO precision has been studied in great detail for a large number of processes, see Tab. 2 for an overview. In many cases, additional jet multiplicities are merged at LO accuracy on top of the highest multiplicity at NLO, and approximate EW corrections can be included for almost every process, see Sec. 2.5 and Fig. 8. The availability of such corrections is only limited by computational resources and has been accomplished, for example, for $W + \{\leq 9\}$ jets [198], $H + \{\leq 7\}$ jets [199] and – in combination with VINCIA – for VBF Higgs production $+\{\leq 4\}$ jets [200]. It has also been used to compute observables in neutral-current DIS at HERA with up to 5 jets in the final state [201]. Further, the multijet merging technology has been extended to loop-induced processes at LO accuracy, MEPS@LOOP^2, in [52,53,55,176], which is of particular relevance for diboson processes at the LHC.

2.4.4 Combining four- and five-flavour calculations: fusing

The merging method described in Sec. 2.4.3 is a well established algorithm to describe multijet observables with NLO accuracy within an inclusive calculation. Originally, the algorithm was limited to the case of massless quarks in the hard scattering matrix element. Although this is a useful approximation in cases where the quark mass is small compared to the typical scales of the observables in question, quark masses often play an important role. Using a scheme with five active quark flavours (5FS) does not allow the use of fixed-order matrix elements to correct the parton-shower resummation in the regions of collinear $g \to b\bar{b}$ splittings. Conversely a scheme with 4 active flavours, (4FS) and massive b-quarks can provide consistent fixed-order predictions in this region, but lacks the resummation of b-jet production at high energies.

A four-flavour scheme simulation of processes involving b-quarks creates additional complications. Experimental analyses involving heavy flavour final states rely on precise simulations involving light jets since these may fake b-quark-initiated jets in detectors. Consequently, both the 4FS and 5FS simulations have to be used simultaneously and their overlap needs to be removed. To overcome this problem, the "fusing" approach [187] has been developed. It rigorously incorporates matrix elements with massive b-quarks into the existing merged predictions while keeping all resummation features and avoiding double counting. In this approach, the hardest heavy-flavour emissions stem from 4FS matrix-element calculations supplemented by Sudakov form factors ("direct" component), whereas softer b-quarks and light jets are still produced by the 5FS multijet matrix elements and the parton shower ("fragmentation" component).

Similar to the FONLL method [202], we need appropriate counter-terms to treat the 4FS matrix elements within a prediction using 5FS PDFs and a 5FS running α_s. In fusing calculations with SHERPA, these are provided as event weights, such as to make the massless multijet event generation usable both inclusively or as a fragmentation component. Applications of SHERPA's fusing implementation have been published for Z + heavy flavour [187] and $t\bar{t}$ + heavy flavour [188] final states.

2.5 Approximate electroweak corrections

Full NLO EW calculations are available with SHERPA for fixed-order calculations only. Nonetheless, approximate higher-order electroweak corrections can be included in particle-level event generation, including parton showering and hadronisation, using the EW virtual ($\mathrm{EW_{virt}}$) scheme, or alternatively through EW Sudakov ($\mathrm{EW_{sud}}$) logarithms. Formally, both correction schemes evaluate the same logarithms, up to NLL, that dominate the electroweak corrections in the high-energy regime, but they differ in the inclusion of finite terms. Both schemes offer the possibility to exponentiate the corrections, resulting in an approximate resummation that estimates the electroweak corrections beyond $\mathcal{O}(\alpha)$ [203].

In practical terms, the two schemes differ in their availability and computational overhead. To fully benefit from their respective advantages, samples with $\mathrm{EW_{virt}}$ and $\mathrm{EW_{sud}}$ corrections can be combined *a posteriori* [55]. The effect of the corrections is usually given via alternative event weights in the output event sample, see Sec. 2.10.2, which allows to compare the corrected predictions with the baseline (QCD only) result. In the following, we discuss the details of the two approximation schemes.

2.5.1 EW virtual approximation

The electroweak virtual approximation ($\mathrm{EW}_{\mathrm{virt}}$), introduced in [184,204], calculates approximate electroweak and subleading mixed QCD-EW corrections which can be incorporated in MC@NLO-matched simulations, including MEPS@NLO multijet merged ones. It supplements the MC@NLO $\overline{\mathrm{B}}$-function with an EW correction built by using exact NLO EW renormalised virtual corrections as well as approximated NLO EW real-emission corrections integrated over their real-emission phase space, either in an additive, multiplicative, or exponentiated manner [55, 171]. The correct electroweak input-parameter and renormalisation scheme dependence is preserved by construction [55, 184].

This approximation reproduces the exact NLO EW corrections in regions with large momentum transfers that are dominated by virtual weak-boson exchanges and renormalisation corrections. The integrated real-photon emission part of the electroweak correction, of particular importance for leptons in the final state, can reliably be recovered by including a soft-photon resummation [205], see Sec. 2.6.

2.5.2 EW Sudakov approximation

The electroweak Sudakov approximation ($\mathrm{EW}_{\mathrm{sud}}$) comprises the leading-logarithmic corrections induced by EW higher orders in the strict high-energy limit. At one-loop, these have been derived by Denner and Pozzorini [206, 207], and implemented in a fully automated and process independent way for the first time in SHERPA [55, 208]. Similar implementations are also available in aMC@NLO [209, 210] and OPENLOOPS [211]. In the high energy limit, the leading higher-order corrections factorise and can be computed by taking ratios of tree-level diagrams, which, in turn, can be evaluated using SHERPA's internal ME generator COMIX. The strength of this approach is twofold: not only does it reproduce the leading and next-to-leading behaviour of higher-order EW corrections, but it also allows the user to combine this prediction with the existing QCD technology, such as parton showering and multijet merging. For details on how to enable SHERPA's EW Sudakov calculations, see App. A.

In practical terms, which energy range corresponds to the high-energy regime depends on the process and the observable, and can be controlled by the user. Intermediate resonances, such as $Z \to \ell^+\ell^-$ within $pp \to \ell^+\ell^- +$ jets processes, formally spoil the high-energy limit, as they are associated with moderate scales of the order of the resonant particle's mass. The implementation in SHERPA disentangles resonant (associated with scales of the order of the resonant mass) and non-resonant (potentially associated with resonance-independent large scales) topologies using the algorithm described in Sec. 2.6.2. If a resonant decay has been identified and clustered, EW Sudakov corrections are computed for the clustered process.

In addition, various subleading contributions can be included to extend the range of validity of the approximation. To be precise, we allow for both the inclusion of logarithms of ratios of invariants which are not formally large, as well as the inclusion of purely imaginary phases appearing when considering $2 \to n$ processes with $n > 2$. These two types of terms were shown to be non-negligible in some cases [209]. While logarithms of ratios of intermediate invariants are not strictly controlled by the $\mathrm{EW}_{\mathrm{sud}}$ approximation, they can be used as either a way to estimate the uncertainty of the approximation or as a way to extend it to lower energies. It is thus advised to include them when comparing to the full NLO EW corrections. On the other hand, the purely imaginary phases should always be included, which is the default.

In the left panel of Fig. 8 we compare the fixed-order exact NLO EW to both the $\mathrm{EW}_{\mathrm{virt}}$ and $\mathrm{EW}_{\mathrm{sud}}$ approximations, including final-state QED radiation corrections in the YFS soft-photon resummation of Sec. 2.6.1 in the setup described in [55]. We find excellent agreement that extends well beyond the strict high-energy limit. The naïvely exponentiated Sudakov logarithms can be used to estimate the size of the $\mathcal{O}(\alpha^2)$ corrections. Unlike the fixed-order NLO EW calculation, both approximations allow their direct incorporation in the QCD parton-shower-matched and multijet-merged machinery of SHERPA. We show their impact in the centre and right panels of Fig. 8, and find that both approximations agree well with each other, indicating a robust prediction. The right panel, however, also exhibits a limitation of the computationally intensive $\mathrm{EW}_{\mathrm{virt}}$ approximation – it is often not available for the higher multiplicities. Here, the $\mathrm{EW}_{\mathrm{sud}}$ approximation, being entirely based on tree-level diagrams, can provide support to all relevant multiplicities and calculate the corresponding EW corrections.

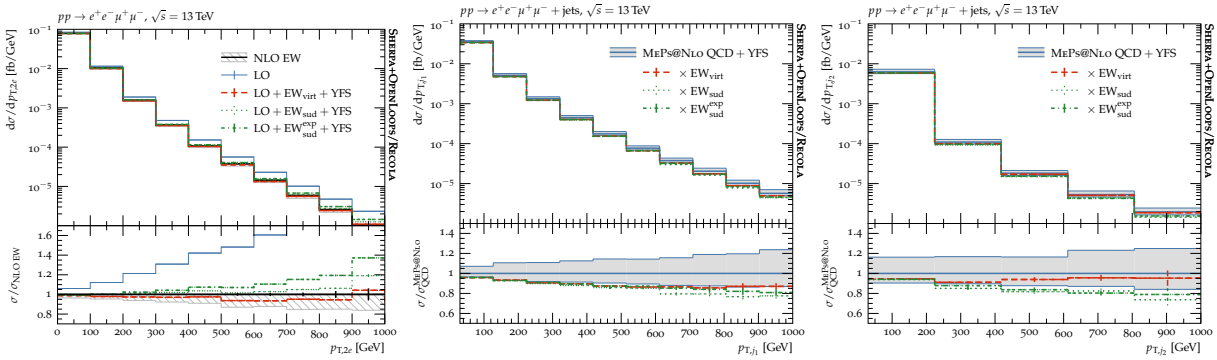

Figure 8: Effects of higher-order EW corrections and their approximations for four-lepton production in the setup of [55]. Left: We show a comparison between exact NLO EW corrections, the EW_{virt} and the EW_{sud} approximations at fixed order in QCD. Both approximations reproduce the EW corrections in the high-energy limit well. Centre and right: We show a MePs@Nlo QCD multijet-merged calculation including either the EW_{virt} or EW_{sud} approximations for higher-order EW corrections. It is important to note that, as seen in the right panel, as the implementation of both approximations differs in the treatment of the lower-multiplicity Mc@Nlo $\mathbb{H}$- and higher-multiplicity LO-events, the two results may differ when these event types have a sizable contribution.

2.6 QED radiative corrections

Sherpa calculates higher-order QED corrections using the soft-photon resummation of Yennie, Frautschi and Suura (YFS) [212]. The YFS formalism uses the universal structure of real and virtual soft-photon radiation, constructing an all-orders approximation that retains all relevant mass effects. Two implementations exist within the Sherpa framework, with Photons [213], detailed in Sec. 2.6.1, focusing on higher-order corrections to particle decays, while Yfs [38], see Sec. 2.6.4, implements corrections to incident leptons as well.

2.6.1 Soft-photon resummation for particle decays

QED final-state radiation is implemented in the Photons [213] module of Sherpa, based on the YFS soft-photon resummation algorithm [212]. To improve its accuracy away from the soft-photon limit, i.e. for hard photon radiation, universal spin-dependent hard collinear emission corrections are applied by default. For dedicated decays, $\tau \to \ell\nu_\ell\nu_\tau$ and some hadron decays [213–215], exact NLO QED corrections are available. NLO QED + NLO EW and NNLO QED + NLO EW corrections are implemented for $W \to \ell\nu$ as well as $Z \to \ell\ell$ and $h \to \ell\ell$ [216], respectively, where the highest precision is needed. Care has to be taken, however, when final states contain multiple competing resonances. This is the topic of Sec. 2.6.2.

In order to not interfere with the QCD parton showering, YFS soft-photon resummed higher-order QED corrections are only applied to decay processes that do not involve coloured particles. An alternative prescription using a collinear factorisation picture exists in the form of a QED parton shower [121] in the CSShower, see Sec. 2.3.1. While this method allows for co-evolving QED and QCD splitting functions, this co-evolution needs only to be considered if QED emissions off quarks are relevant. In addition, currently it lacks both the soft-photon coherence inherent in the YFS soft-photon resummation and the dedicated higher-order corrections.

2.6.2 Resonance identification

Complex final states often contain (multiple) internal resonances. Thus, additional care is required when effecting higher-order QED corrections in order to preserve these structures. To this end, Sherpa employs a universal resonance identification algorithm [61]. First, all possible resonances occurring in the chosen model are identified by scanning the final state of a scattering process for possible recombinations into resonant states. Second, all such combinations are ordered in increasing distance from the nominal on-shell

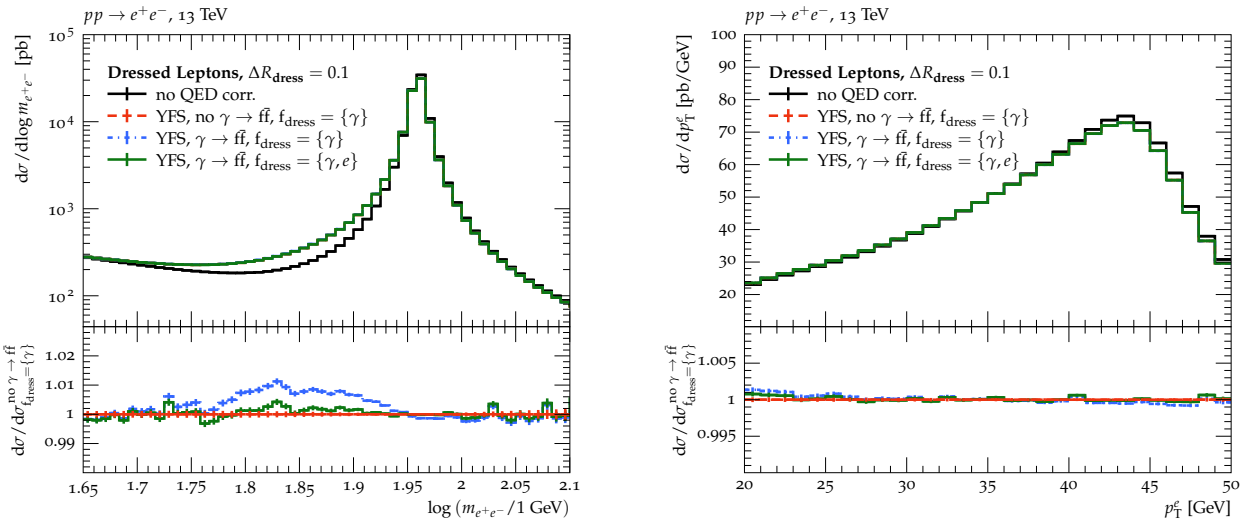

Figure 9: The dressed dilepton invariant mass $m_{e^+e^-}$ (left) and electron transverse momentum p^e_T (right) in Drell–Yan production as described at leading order (black), by the YFS soft-photon resummation at YFS+NLO QED+NLO EW accuracy without photon-splitting corrections (red) or additionally resolving the photons further into pairs of charged particles (blue and green), including mitigating effects of adequately improved dressing strategies. For details see [217].

resonance in units of its width, using $\Delta = |m^{\text{inv}}_{\text{kin}} - m_{\text{res}}|/\Gamma_{\text{res}}$. Starting with the recombination with the smallest Δ, resonances are identified as present in the current configuration, and recombination candidates with $\Delta > \Delta_{\text{thr}}$ are classified as non-resonant. Identified resonances are treated separately, ensuring that no momentum is transferred outside a resonant-decay system through the application of higher-order QED corrections. Finally, all non-resonantly produced final states are corrected using the universal YFS soft-photon resummation together with the universal hard-collinear corrections.

2.6.3 Photon-splitting corrections

A feature of higher-order QED effects absent in the YFS soft-photon resummation are photon-splitting corrections. To account for these effects, SHERPA's PHOTONS module has been extended with PHOTONSPLITTER [217]. Despite being of relative $\mathcal{O}(\alpha^2)$ and only enhanced by single collinear logarithms compared to the Born configuration, these corrections can play an appreciable role when hard primary photons split into pairs of light charged particles. The possibility for a photon to be replaced by an electron or muon pair also has important consequences for lepton dressing. This module therefore allows photons to split into electrons, muons and/or light charged hadrons (the relevant QCD degrees of freedom at this energy) in a parton-shower-like collinear evolution, starting from the primary photon ensemble generated by YFS. Figure 9 shows the impact of photon-splitting corrections on Drell–Yan electron-pair production at the LHC, including their mitigation using a modified lepton dressing procedure. For details see [217].

2.6.4 Soft-photon resummation for e^+e^- colliders

At lepton–lepton colliders, an important source of uncertainty which must be included is the modelling of photon emissions in the initial state. Such emissions can spoil the perturbative expansion as they lead to potentially large logarithms, which arise from the emission of soft and/or collinear photons. To ensure the stability of theory predictions, and to reduce the overall uncertainty, these logarithms must be resummed. SHERPA currently supports two different approaches to the treatment of QED ISR. The first approach uses the electron structure function, which is a solution of the DGLAP evolution equations [218–221] using LO initial conditions [222], see Sec. 2.1.2. This analytic approach can be combined with a traditional parton shower, extended to QED [121], to generate exclusive kinematic distributions for the collinear photons. In the second approach, we use the YFS theorem [212] to resum the emission of soft photons to all orders in α. In this method, the photon emissions are considered in a fully differential form where the photons are

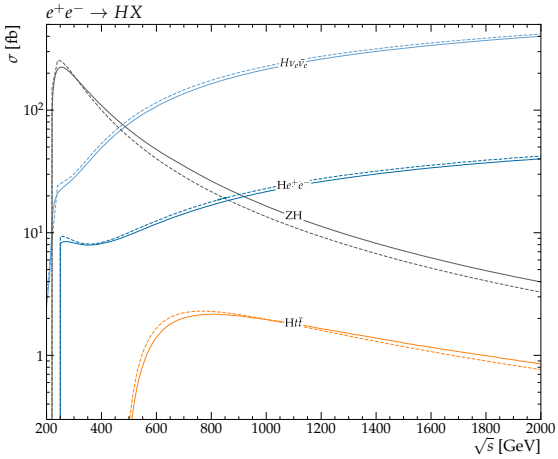

Figure 10: Total cross section for $e^+e^- \to HX$ at the Born level (dashed) and with ISR (solid) corrections included.

explicitly created and the treatment of their phase space is exact.

The YFS approach was originally implemented in process-specific Monte Carlo tools [223–226] that were predominantly used for the LEP physics programme and were crucial for its electroweak precision measurements [227]. Despite these tools still being available and being further developed, having a process-independent Monte Carlo event generator based on the YFS formalism is highly desirable. Hence, while such a YFS-based implementation for QED FSR for arbitrary final states was available for some time, see Sec. 2.6.1, this framework has been extended to include QED ISR for initial-state leptons in a process-independent fashion in [38]. Therein, corrections related to hard collinear photon emissions are available in a leading-logarithmic formulation up to $\mathcal{O}(\alpha^3 L^3)$. An automated calculation of the complete fixed-order corrections at full NLO EW accuracy is envisioned for future SHERPA versions. As an example application, we present a number of Higgs production cross sections in Fig. 10 as a function of the collider centre-of-mass energy.

2.7 Multi-parton interactions

Multi-parton interactions (MPIs) have long been established as an important physics model for collider event simulation which ensures that particle production, and its scaling behaviour with the hadronic centre-of-mass energy, are correctly described [228]. The SHERPA model for this effect builds on the original Sjöstrand–van Zijl approach [228]. While newer versions of PYTHIA integrate the secondary scatterings into the initial-state parton evolution [229, 230], and add final-state parton showering as well as hadronic rescattering effects [231], SHERPA treats the scatterings as independent, apart from momentum-conserving and colour reconnection effects. The perturbatively computable (regularised) parton-level cross section is normalised to the non-diffractive hadron-level cross section and exponentiated in an expression similar to a Sudakov factor. This expression is used to generate a sequence of secondary interactions, which individually undergo parton-shower evolution in the initial and final states. The production of the secondary interactions is integrated into the multijet merging algorithm used to describe the hard scattering [232].

As a new feature in version 3, SHERPA is now capable of modelling multiple scattering effects in processes with resolved photons. It is also now possible to veto additional scatters between beam particles, which is useful in measurements of large rapidity gaps and diffractive jet production [163], for example. In this way, survival probabilities can be computed as the probability for no further scatters to occur, akin to their estimation in [233–235].

2.8 Hadronisation

The transition from the region where QCD partons are asymptotically free to the regime where they are bound into hadrons is the traditional domain of Monte Carlo event generators. This region cannot be

described using first-principles calculations due to the complications of the transition from the perturbative to the non-perturbative regime of the theory. A number of models, which are rooted in a few theoretically calculable quantities and experimental observations, are therefore employed. The ones used in SHERPA are described in this section.

2.8.1 Beam remnant handling

In collisions involving hadronic initial states, one or more partons are typically extracted from the incoming beam particles. This is modelled via the perturbatively described hard scattering and the perturbatively modelled, but softer, multi-parton interactions, see Secs. 2.2 and 2.7. Both types of calculations are dressed with the parton showers of Sec. 2.3 which ultimately terminate at low transverse-momentum scales of around 1 GeV.

The breakup of incoming hadrons (and other beam particles with substructure), and the formation of the beam remnants, begins with a list of shower initiators from the above perturbative descriptions. The breakup of incoming particles is guided by flavour compensation, colour compensation, longitudinal momentum distribution according to the PDFs, and transverse momentum distribution according to a polynomially-suppressed Gaussian. In addition, the valence structure of the beam particle is respected; in particular, baryons are considered to constitute a valence quark-diquark pair. Details on this model can be found in App. C.

2.8.2 Colour reconnections

The partons produced by the hard scattering and multi-parton interactions, their subsequent parton showers, and the break-ups of the beam remnants all turn into so-called primary hadrons. These primary hadrons have their colours assigned in the large-N_c limit. This means that effectively, at this stage, every colour in the parton ensemble has exactly one anti-colour and vice versa. The difference between the $N_c \to \infty$ approximation and the actual value $N_c = 3$, and the existence of potential soft non-perturbative gluon interactions (so-called "gluers" [236]), suggests that this model can be improved by a rearrangement of the original colour assignments of the partons. In particular, the non-perturbative nature of the long-range strong interactions introduces significant liberty in the modelling of such colour reconnections (CRs).

The model in SHERPA incorporates various ideas from earlier literature [228, 229, 237–247]. Assuming that N different colours (matched by exactly N anti-colours) emerge from the scatters, showers, and beam remnants, the model checks N^2 times for possible colour reassignments. In each such attempt, two colours i and j are randomly chosen and the relative distances d of the corresponding parton pairs $\langle i\bar{i}\rangle$ and $\langle j\bar{j}\rangle$ and the swapped pairs $\langle i\bar{j}\rangle$ and $\langle j\bar{i}\rangle$ is calculated. For each pair kl, the distance in momentum space is given by $d_{kl} = \log(1 + (p_k p_l - m_k m_l)/Q_0^2)$. Based on this distance, a colour reassignment happens with a probability given by $P_{\text{swap}}(i \leftrightarrow j) = R_c\{1 - \exp[\eta_Q\,(d_{i\bar{i}} + d_{j\bar{j}} - d_{i\bar{j}} - d_{j\bar{i}})]\}$. In these equations, Q_0 is the infrared scale in the distance measure, R_c is the colour factor, and η_Q is the weight of the distances in the exponential. The (untuned) defaults are $Q_0 \approx 1$ GeV, $R_c \approx 1/9$, and $\eta_Q \approx 0.1$.

2.8.3 Cluster hadronisation

SHERPA's default hadronisation model [248,249] is based on the twin concepts of local parton-hadron duality (LPHD) [250] and preconfinement [251–253], which postulate that the flow of quantum numbers, momenta, and energies at the hadron level closely follows their counterparts at the parton level, and that the transition from partons to hadrons proceeds through the formation of colourless clusters with a *perturbatively* calculable mass spectrum. The first realisation of the LPHD paradigm in the form of the Feynman–Field independent fragmentation model [254] suffered from a range of theoretical issues, among them lack of Lorentz invariance. These issues were ultimately resolved by the concept of preconfinement, which introduced the intermediate step of a non-perturbative splitting of gluons into quark–anti-quark pairs [255, 256] and the subsequent formation of colour-neutral clusters and their decay into hadrons [257]. The first cluster fragmentation model embedded in a widely used event generator, HERWIG [4, 258], was introduced shortly afterwards [109, 259] and is continuously improved [3, 260, 261].

SHERPA's cluster model [248, 249] differs from the HERWIG model in multiple ways. Firstly, SHERPA does not introduce non-perturbative gluon masses but rather keeps the gluons massless, and allows not only light

up and down quarks, but also strange quarks and diquarks as decay products of their forced splitting at the onset of hadronisation. This results in the presence of baryonic clusters throughout the hadronisation process. Secondly, the fission of relatively heavy clusters into two lighter ones is not parametrised by selecting masses of the latter in (typically) isotropic decays; instead, SHERPA distributes light-cone momentum fractions of the new clusters with respect to the constituents of the decaying cluster according to "fragmentation functions", and applies a Gaussian transverse momentum distribution to the decay kinematics. Finally, there are also differences in the treatment of binary cluster decays into primary hadrons, including kinematics and the way the hadron species are selected. Overall, despite the footing of both models in the same underlying physics assumptions, these differences result in a manifestly different hadronisation model with different sets of critical parameters that need to be tuned to data.

2.8.4 Alternative hadronisation model via interface to Pythia 8

An alternative approach to hadronisation is provided by the string picture of QCD [262–264] which builds on the observation of a potential between colour charges that increases linearly with their position-space distance[†]. The potential is represented by one-dimensional strings, which carry a finite energy density per unit length. As the strings are "stretched" with the partons moving away from each other, their stored energy allows the dynamic creation of quark–anti-quark pairs, akin to the Schwinger mechanism in QED [267, 268], essentially breaking the string into smaller, lighter fragments. Successive refinements, including symmetrising the string fragmentation function whilst respecting Lorentz-invariance and causality [269], extending the model beyond the simple case of strings spanned by quark–anti-quark pairs and including the effect of gluons [270, 271], and the modelling of baryon production [272], have contributed to establishing the Lund model [273, 274] as probably the most phenomenologically successful hadronisation model.

SHERPA provides an interface to the Lund model implemented in PYTHIA 8 [6, 275]. See App. A for instructions to enable it. The support for both cluster hadronisation and string fragmentation available in SHERPA allows for direct comparisons of hadronisation models and their observable effects, due to the identical treatment of the perturbative phase of the event.

2.9 Hadron decays

The SHERPA framework contains a built-in module handling hadron and tau-lepton decays [276, 277]. It contains decay tables with branching ratios for approximately 2500 decay channels, many of which have their kinematics modelled according to a matrix element with corresponding form factors. In particular, decays of the tau lepton and heavy mesons have form-factor models similar to dedicated codes like TAUOLA [278] and EVTGEN [279].

Several additional features are implemented: spin correlations can be enabled to account for the correlation of the helicity of an unstable particle between the production and decay matrix elements. Neutral meson mixing can be described, including advanced features like CP violation in the decay, in the mixing, and in the interference between them [2]. Decay kinematics are adjusted to account for the finite-width Breit–Wigner line shape of the decaying particle. QED radiation can be simulated from all charged particles involved in the hadron decay cascade within the formalism and implementation described in Sec. 2.6. Aliases can be defined and used for a fine-tuned correlated steering of open decay channels. For hadrons with incomplete exclusive decay tables, these can be completed by using the decays of their partonic content, corrected for higher-order QCD effects using the parton shower of Sec. 2.3, and subsequent hadronisation to yield a description of the missing decay channels.

2.10 Event generation results and variations

After all stages of the simulation of a collider event have been completed, the event exists as an internal representation of flavours, momenta, weights and weight components. We describe in this section how this information can be further processed and stored in standardised output formats.

[†]Approaches to combine the respective benefits of string and cluster hadronisation [265, 266] have not been followed up in the past decades, arguably because they have not been provided in the form of a widely used event generator.

2.10.1 Weighted vs. unweighted event generation

SHERPA events are produced as tuples $\{\Phi_i, w_i, n_{\text{trial},i}\}$, wherein the phase-space point Φ_i encodes the flavours and momenta of all involved particles constituting this event. All such events initially have a probabilistic Monte Carlo weight w_i associated with them, which must be taken into account when calculating expectation values for observables,

$$\langle O \rangle = \frac{1}{N_{\text{trial}}} \cdot \sum_{i=1}^{n} w_i \left(\Phi_i\right) O\left(\Phi_i\right) , \quad \text{with} \quad N_{\text{trial}} = \sum_{i=1}^{n} n_{\text{trial},i} \, . \tag{2.1}$$

Therein, $O\left(\Phi_i\right)$ is the value of the observable under consideration, and $n_{\text{trial},i}$ is the number of trials needed to successfully generate event Φ_i, and N_{trial} is their total sum. In essence, N_{trial} keeps track of all attempts that resulted in a weight $w_i = 0$ during any stage of event generation to retain the correct sample normalisation without the need to write out events that will not contribute to any observable.

In applications with expensive post-processing steps of the event sample, for example a full detector simulation, or if storage is a concern, it is favourable to minimise the number of events in the sample without reducing its statistical power. This is achieved by an unweighting step, which accepts or rejects events in accordance with their probabilistic weight. The resulting sample consists of the accepted events only, and their event weights are all normalised to a constant weight while n_{trials} book-keeps the rejected events. Exceptions from such a uniformly-weighted sample exist for events with particularly large weights or if a non-uniform bias is applied to the event generation. For further details, we refer the user to the full user manual distributed with the SHERPA code.

Applying the unweighting step as described above is the default behaviour of SHERPA. Since the fraction of events that survive the unweighting is typically very small, deferring computations that do not affect the weight until after accepting an event gives rise to major speed-ups of the overall event generation. In [23], we have introduced a pilot-run strategy leading to an overall reduction in computing time by about a factor of forty for typical simulation setups used by the LHC collaborations.

2.10.2 On-the-fly uncertainty estimates

During event generation, SHERPA can calculate a variety of alternative event weights for various physical and algorithmic variations. For each alternative weight, its fraction of the nominal weight encodes the probability of the event to happen for that variation. This multi-weight handling removes the need to produce dedicated event samples for each variation separately, for example to estimate an uncertainty on the nominal prediction. Furthermore, downstream processing steps such as physics analyses or detector-response simulations only need to process a single event sample and still retain all variations by simply propagating through the alternative event weights. The additional spread in weights which occurs when using this method, and the resulting reduced statistical power of the event-weight sample, is usually far outweighed by the benefits of the method, i.e. strongly reduced computing and storage needs. Similar techniques are used in the VINCIA [280], PYTHIA [281] and HERWIG [282] event generators. For PYTHIA, an extension of the approach to hadronisation models has recently been presented [283].

For QCD uncertainty estimates, SHERPA supports factorisation and renormalisation scale variations, as well as PDF variations [284]. To give some application examples, this allows one to quantify 7-point scale variation uncertainties, study the spread of predictions due to different PDF fits by different fitter groups, and/or derive the PDF uncertainty for each PDF set individually. The strong coupling value for $\alpha_s(m_{\text{Z}}^2)$ is usually taken from the PDF set (and can thus be varied by selecting PDF sets with different inputs for $\alpha_s(m_{\text{Z}}^2)$), but it can also be varied independently of the PDF. By default, all such QCD parameter variations are applied to both the hard process and the parton shower simultaneously. Nonetheless, SHERPA will additionally report variation results for the hard process only.

The approximate EW corrections discussed in Sec. 2.5 are usually also given as alternative event weights, allowing the user to compare the effect of including the corrections with the baseline prediction [55]. The same applies to the components of the heavy-flavour matching discussed in Sec. 2.4.4. Finally, on the algorithmic side, as of SHERPA 3 one can vary the merging parameter, Q_{cut}, on the fly when generating multijet-merged event samples, see Sec. 2.4.3. This allows the user to study the effect of this formally higher-order variation, e.g. to confirm that its impact is small compared to other uncertainties in the phase space relevant for the analysis at hand.

Ultimately, SHERPA reports the total cross section not only for the nominal scale and input parameter choices, but also for each requested variation thereof. These alternative sample cross sections are passed to the HEPMC [285, 286] event output or directly to the RIVET analysis framework [287, 288] via SHERPA's internal interface. SHERPA follows the naming conventions for event-weight variations specified in [89].

2.10.3 Storing and analysing events

As already mentioned, SHERPA provides interfaces to the HEPMC and RIVET libraries, which can be used to facilitate the analysis of its output. Generally, HEPMC serves as a common event-record format, allowing SHERPA to export its generated events in a standardised manner and ensuring compatibility with likewise standard-compatible analysis tools and frameworks. HEPMC itself supports a variety of structured formats for storing the Monte Carlo event record to disk. SHERPA supports HEPMC version 3 onwards [286].

RIVET [287–289] is a common analysis toolkit for the validation of Monte Carlo event generators using experimental data. It uses the Monte Carlo events in the HEPMC format as an input, either reading the event record from file (independently of which generator produced the events), or passed programmatically as an object when a dedicated interface is in place. SHERPA supports both options, where its dedicated interface is supported from RIVET version 3 onwards. Starting with RIVET version 4 [288], SHERPA supports the serialisation of the RIVET output, allowing for efficient data reductions in memory as part of MPI-collective communications in high-performance applications. This avoids the need for *a posteriori* merging of histogram files entirely. Note that both HEPMC 3 and RIVET 3, as well as later versions, have native multi-weight support, which makes it very straightforward to plot uncertainty bands via RIVET when using SHERPA multi-weight event samples as an input.

RIVET can also be used to fill cross-section interpolation grids from SHERPA's fixed-order calculations. This can be achieved using a RIVET plugin called MCGRID [290,291] that projects individual events on differential observables and produces corresponding interpolation grids in the APPLGRID [292] or FASTNLO [293] format. These grids can be used for the fast and flexible evaluation of scale, α_s, and PDF variations in leading- and next-to-leading-order QCD calculations. The required event information is provided by SHERPA via auxiliary event weights.

For instructions on enabling SHERPA's HEPMC and RIVET interfaces and its MPI support, see App. A.

3 Development pipeline

In this section we briefly describe software and physics projects that have been developed in the SHERPA framework, but are not yet publicly released with SHERPA 3.0 or 3.1. They represent feature candidates to be included in near-future versions of the package.

3.1 CAESAR resummation with SHERPA

The SHERPA framework can be used to perform semi-analytic QCD resummation calculations in the CAESAR formalism [294, 295], allowing for the all-orders inclusion of leading and next-to-leading logarithms in the observable value for suitable variables. The original implementation of the CAESAR plugin to SHERPA was presented in [296]. It utilises the event generation framework, with SHERPA facilitating all the process management, providing access to matrix-element generators, performing phase-space integration, and providing event-analysis functionality. In the context of matching the resummation to fixed-order calculations, aiming for NLO+NLL' accuracy, the SHERPA implementation of the Catani–Seymour dipole subtraction and the interfaces to the one-loop providers RECOLA and OPENLOOPS are employed. To correct the resummed predictions for non-perturbative corrections from the underlying event and hadronisation, multi-differential transfer matrices, derived from corresponding SHERPA simulations, can be employed, capturing the kinematical migration of parton-level to particle-level events [297–299].

The CAESAR implementation of SHERPA has been used to derive resummed predictions for soft-drop thrust [297] in the context of extractions of the strong coupling constant [300] and multijet resolution scales [165] in electron–positron annihilation, as well as NLO+NLL' accurate predictions for soft-drop groomed hadronic event shapes [167], and jet angularities in proton–proton collisions at the LHC [298, 301, 302] and RHIC [299]. Recently, it was applied to plain and groomed event shapes in neutral-current

deep inelastic scattering [166, 303–305], as well as event-shape observables in hadronic Higgs-boson decays at a future lepton collider [306].

3.2 Precision resummation with SCET in SHERPA

In addition to the CAESAR resummation calculations described above, a number of targeted highest-accuracy resummation calculations were performed in the SCET formalism [307, 308] using the SHERPA framework. These calculations make use of a purpose-built resummation routine which is interfaced to SHERPA. In this setup, SHERPA supplies the exact fixed-order matrix elements, using the interfaces to one-loop providers (see Sec. 2.2.2) and the inbuilt Catani–Seymour dipole subtraction, and carries out the matching to the resummation away from the infrared limits. SHERPA also handles the phase-space integration.

This has allowed the calculation of a number of selected observables at high fixed-order and resummed precision. For example, the double-differential q_T–$\Delta\phi$ spectrum in both charged- and neutral-current Drell–Yan production, as well as the ratio thereof, were calculated at $N^3LL'+N^2LO$ accuracy, including the non-negligible top-mass-dependent singlet contributions [309]. Further, these developments have been used to calculate various observables in $t\bar{t}$ production. Away from the $t\bar{t}$ production threshold, the projected transverse momentum distributions were calculated at approximate $N^2LL'+N^2LO$ accuracy [310]. In the entire $t\bar{t}$ production region, including the threshold region, the q_T and $\Delta\phi$ spectra were calculated at N^2LL+N^2LO [311]. The q_T spectrum of Higgs production in gluon fusion was calculated at subleading power (up to N^2LP) at NLO in [312]. This high-precision resummation interface will be provided in future versions.

3.3 High-performance and heterogeneous computing

SHERPA is one of the workhorses of the modern experimental simulation toolchain, in particular for the LHC experiments. While the code provides enhanced physics modelling capabilities based on high-multiplicity multijet merged simulations, the required matrix element calculations often strain the experimental computing budgets [313–316]. To reduce the computing footprint and still facilitate cutting-edge physics simulations, SHERPA has undergone extensive performance improvements in the past years [23, 71, 147]. These have been described in Secs. 2.1.2, 2.2 and 2.10.1, and have also been backported to the SHERPA v2.2 series, resulting in significant event generation speed gains for the traditional compute model of running SHERPA on a single CPU core.

The current trend towards very large (exascale) HPC clusters, and towards an increasing reliance on offloading computations to GPU-like accelerator hardware, brings about new challenges. Large HPC clusters usually rely on parallel file systems (e.g. Lustre). To take full advantage of such a file system, one also needs to parallelise input/output operations. On the other hand, using a GPU usually requires reorganisation of the data in memory, copying data to and from the GPU, and compiling the compute kernel code for the given GPU architecture, thus requiring extensive changes to existing codebases like SHERPA.

To improve performance on parallel file systems, future versions of SHERPA will include the `LHEH5` interface described in [198,199]. When SHERPA is run in parallel mode via MPI, the `LHEH5` technology enables efficient parallel I/O operations across many nodes. This technology also provides the means to store parton-level events at leading and next-to-leading order, which can be used for multijet merged simulations within SHERPA or PYTHIA. This provides new options to cross-check simulations with different parton showers or hadronisation modules, in order to derive systematic uncertainty estimates. In addition, SHERPA now employs more efficient computing strategies, including the recycling of particularly intensive parts of the simulation, where possible.

The `LHEH5` interface will also ease the use of GPU resources, as it allows SHERPA to read in parton-level events from different matrix element generators, such as the GPU-enabled simulation program PEPPER [317–320]. The excellent MPI performance of SHERPA is further enhanced by the introduction of a RIVET 4 [288] and YODA 2 [321] interface, allowing for an efficient in-memory merging of results across MPI nodes (see Sec. 2.10).

3.4 Machine learning for phase-space sampling and event unweighting

Within the SHERPA framework, several applications of modern machine learning techniques are being explored with the aim of further improving the generator performance. The focus is currently on the hard

event component; in particular, on achieving the efficient sampling of high-dimensional phase spaces. This involves the generation of momentum configurations distributed according to the desired squared matrix element, and the efficient unweighting of events.

We have pioneered the development of novel sampling algorithms which work by remapping the integration variables using trainable Normalising Flows [319, 322, 323]. The task of optimising the performance of the process-specific multi-channel importance sampler is traditionally accomplished with the VEGAS algorithm [324]. However, VEGAS assumes a factorisable target distribution, which is typically not found in multi-particle transition matrix elements and the phase-space parametrisations which are employed, limiting the potential for further optimisations. Normalising-flow maps are more flexible and facilitate a better optimisation of the sampling distribution to the true target functions. As a result, the statistical variance of cross-section predictions can be significantly reduced for many processes.

In general, event unweighting (the generation of events with unit weight) is a rather inefficient process, especially for high-multiplicity processes, due to the large spread in event weights. Unweighting efficiencies for these processes often fall below the permille level [198]. At the same time, the required matrix element evaluations are computationally costly. To improve the efficiency of this process, we have developed a novel two-stage unweighting algorithm. It relies on a fast neural network surrogate for the event weight in an initial unweighting phase, followed by a second rejection sampling against the true event weight [325]. The resulting event sample is unbiased and follows the desired distribution, though statistically somewhat diluted due to the possible appearance of overweights. However, the effective gain factors turn out to be significant for complex final states. To improve the algorithm's performance, physics knowledge about the target function can be incorporated into the surrogate construction. To this end, we have studied network architectures that reflect the dipole factorisation property of QCD real-emission matrix elements [326], resulting in a performance boost for the new unweighting algorithm [327].

3.5 Neutrino physics interface

The current and next-generation neutrino experiments are entering a precision era, in which the dominant uncertainty will shift from statistical in nature to systematic [328–330], enabling a multitude of analyses that will probe physics beyond the Standard Model. In particular, there has been a push to expand the searches for BSM physics at accelerator neutrino experiments, such as the SBN program [331] and DUNE [328]. SHERPA has proven to be a versatile tool for the corresponding event simulations. To expedite the inclusion of novel models into the experimental pipeline, an interface to the UFO module (see Sec. 2.2.8 for details) has been developed to return only the leptonic current involved [332].

DUNE is expected to measure an unprecedented number of tau neutrino events in the far detector [329]. In the past, neutrino generators have simply assumed that the produced tau lepton is purely left-handed. This has been shown to be a poor assumption [333]. To facilitate the needed precision for DUNE, SHERPA now provides an interface to enable neutrino generators to appropriately include spin-correlations for tau decays [334]. Further, within the neutrino community, only PYTHIA is currently used for estimating the hadronisation of particles in the DIS region [335–340]. Extending the above interface to allow for neutrino generators to use SHERPA for hadronisation will enable a more robust estimate of the uncertainties in this energy region.

4 Conclusions

In this paper, we have described the new major release of the general-purpose Monte Carlo event generator SHERPA, a numerical simulation program designed specifically to cope with the high centre-of-mass energies at CERN's Large Hadron Collider and the associated physics challenges. Over the last few years, SHERPA has been extended to the simulation of a wider range of physics processes, such as polarised cross sections, photoproduction and diffractive jet production. The physics capabilities of the generator have been further enhanced through improved models for soft physics and a universal framework for NLO calculations in the complete Standard Model. In addition to these and the other developments described here, SHERPA also provides a platform for various other precision physics simulations, such as a generic NLL resummation framework and a neutrino event generator. Together with a number of technical improvements, the above developments are released publicly and supported as SHERPA version 3, which will form the basis for further

refinement of the physics models in the eras of the High-Luminosity LHC and the EIC, and for the preparation of other potential future collider experiments.

Acknowledgements

EB, MK and SS acknowledge financial support from BMBF (projects 05H21MGCAB, 05D23MG1 and 05H24MGA) and funding by the Deutsche Forschungsgemeinschaft (DFG, German Research Foundation) - projects 456104544 and 510810461. This research was supported by the Fermi National Accelerator Laboratory (Fermilab), a U.S. Department of Energy, Office of Science, HEP User Facility managed by Fermi Research Alliance, LLC (FRA), acting under Contract No. DE–AC02–07CH11359. AP acknowledges financial support from grant No. 2019/34/E/ST2/004571012 of the National Science Centre (NCN), Poland and also by the Priority Research Area Digiworld under the program Excellence Initiative — Research University at the Jagiellonian University in Krakow. DR acknowledges funding by the European Union under the HORIZON program in Marie Skłodowska-Curie project No. 101153541. MS is funded by the Royal Society through a University Research Fellowship (URF\R1\180549, URF\R\231031) and an Enhancement Award (RGF\EA\181033, CEC19\100349, and RF\ERE\210397) as well as the STFC (ST/X003167/1 and ST/X000745/1). LF is supported by Leverhulme Grant LIP-2021-014. LF and PM acknowledge support from an STFC studentship under grant ST/P001246/1. PM is supported by the Swiss National Science Foundation (SNF) under contract 200020-204200 and acknowledges support from the STFC under grant agreement ST/P006744/1. The work of JI was supported by the U.S. Department of Energy, Office of Science, Office of Advanced Scientific Computing Research, Scientific Discovery through Advanced Computing (SciDAC-5) program, grant "NeuCol". CG acknowledges funding via the SWIFT-HEP project (grant number ST/V002627/1).

A Installing SHERPA

SHERPA is distributed as a tarred and gzipped file named `sherpa-<VERSION>.tar.gz` available from the *Downloads* section of the project's webpage[‡]. The file can be unpacked in the current working directory with the shell command

```
$ tar -xzf sherpa-<VERSION>.tar.gz
```

Alternatively, SHERPA can be accessed via Git, through

```
$ git clone --single-branch -b rel-<VERSION> https://gitlab.com/sherpa-team/sherpa.git
```

In either case, to guarantee successful installation, the following tools should be available on the system:

- a recent C/C++ compiler toolchain,
- a recent version of CMake to configure a build directory,
- and Make or Ninja to build and install SHERPA.

A Fortran compiler is recommended. For the use of UFO models, an installation of Python version 3.5 or later is required. Installations of the LHAPDF and `libzip` libraries are also recommended, but it is possible to let SHERPA install its own copies of both libraries, as will be discussed below.

Compilation and installation proceed through the following standard CMake workflow:

```
$ cd sherpa-<VERSION>/
$ cmake -S . -B <builddir> -DCMAKE_INSTALL_PREFIX=<installdir> [+ config options]
$ cmake --build <builddir> [+ build options, e.g. -j 8]
$ cmake --install <builddir>
```

[‡] `https://sherpa-team.gitlab.io`

Option/package name	Enable option/interface	Specify package location	References
MPI	`-DSHERPA_ENABLE_MPI=ON`	`-DMPI_DIR=<path>`	—
HepMC 3.0.0 or later	`-DSHERPA_ENABLE_HEPMC3=ON`	`-DHEPMC3_DIR=<path>`	[285, 286]
Lhapdf	`-DSHERPA_ENABLE_LHAPDF=ON`	`-DLHAPDF_DIR=<path>`	[19]
McFm	`-DSHERPA_ENABLE_MCFM=ON`	`-DMCFM_DIR=<path>`	[71]
OpenLoops	`-DSHERPA_ENABLE_OPENLOOPS=ON`	`-DOPENLOOPS_DIR=<path>`	[65, 66]
Pythia 8.220 or later	`-DSHERPA_ENABLE_PYTHIA8=ON`	`-DPYTHIA8_DIR=<path>`	[6]
Recola	`-DSHERPA_ENABLE_RECOLA=ON`	`-DRECOLA_DIR=<path>`	[67–69]
Rivet 3.0.0 or later	`-DSHERPA_ENABLE_RIVET=ON`	`-DRIVET_DIR=<path>`	[287, 288]
EW Sudakovs	`-DSHERPA_ENABLE_EWSUD=ON`	—	[55, 208]
Ufo	`-DSHERPA_ENABLE_UFO=ON`	—	[45, 46]

Table 3: Configuration options to enable some of Sherpa's optional features and interfaces to external packages. A package location needs to be specified only if an external package is installed in a non-standard location, or to enforce the usage of a specific installation of the package. The Ufo and EW Sudakovs options do not rely on external packages and therefore have no associated package location option.

where `<builddir>` has to be replaced with the (temporary) directory in which intermediate files are stored for the build process, and `<installdir>` with the installation directory into which the build products are installed. The structure of the program within `<installdir>` is as follows (if the installation procedure is not further customised):

- `<installdir>/bin`: the main `Sherpa` executable and additional auxiliary executables and scripts,
- `<installdir>/include`: headers that define the API to use Sherpa as an external framework from third party tools, and which are used when Sherpa writes out process libraries that must be compiled by the user,
- `<installdir>/lib`: basic library files,
- `<installdir>/share`: PDF data files, tau lepton and hadron decay data, example run cards, command line auto-completion files and other auxiliary files.

Sherpa can be interfaced with various external packages. To enable this, the user has to add the corresponding options to the `cmake` configuration command:

```
$ cmake -S . -B <builddir> [...] -DSHERPA_ENABLE_<PACKAGENAME>=ON
```

where `<PACKAGENAME>` is replaced by the external package name, e.g. `RIVET`, `LHAPDF`, `HEPMC3` etc. If the external package is not installed in a standard location, the user might need to specify the installation directory of the package as follows:

```
$ cmake -S . -B <builddir> [...] -D<PACKAGENAME>_DIR=<package_installdir>
```

In Tab. 3, we list the configuration options to enable interfaces to external packages and optional features which are referred to in this article. However, it is not a complete list of all available interfaces and options. For this, we refer the reader to the manual distributed with the actual code release and can also be found on the Sherpa download webpage. Alternatively, a complete list of possible configuration options can be listed by running `cmake -LA <builddir>` or `ccmake <builddir>`.

B Input cards

When Sherpa is run without any arguments, it scans for a configuration file called `Sherpa.yaml` in the current working directory. Such a configuration file is also called a runcard. It usually defines the process(es) for which events should be generated, the collider setup, and other physics and technical settings the user

```yaml
# set up beams for LHC run 2
BEAMS: 2212
BEAM_ENERGIES: 6500

TAGS:
  NJETS: 4

# request events for pp -> W[ev] with up to four additional final-state jets
PROCESSES:
- 93 93 -> 11 -12 93{$(NJETS)}:
    Order: {QCD: 0, EW: 2}
    CKKW: 20
    # use NLO accuracy for the lowest three multiplicities (2->2, 2->3 and 2->4)
    2->2-4:
      NLO_Mode: MC@NLO
      NLO_Order: {QCD: 1, EW: 0}
      Loop_Generator: OpenLoops
```

Listing 1: An example SHERPA runcard for generating $pp \to e^-\bar{\nu}_e + \text{jets}$ events.

wishes to customise. An example for the production of an electron–neutrino pair with up to four additional jets is given in Listing 1.

The settings in the runcard are given in YAML syntax [341]. In the example, we set up symmetric proton beams corresponding to a collision centre-of-mass energy of 13 TeV, by specifying the single-valued settings `BEAMS: 2212` and `BEAM_ENERGIES: 6500`. Next, we specify a tag using the `TAGS` setting. We call the tag `NJETS` and set it to the value `4`. Any occurrence of `$(NJETS)` in the runcard will now be replaced with that value. Finally, we add a process using `PROCESSES`. This setting also takes a list, since SHERPA can generate events for more than one process. Here, we only add one process, using `93 93 -> 11 -12 93{$(NJETS)}`, which translates to $pp \to e^-\bar{\nu}_e +$ up to four jets. The process specification itself, `93 93 -> 11 -12 93{$(NJETS)}`, takes various subsettings, e.g. the orders in the strong and electroweak couplings using the `Order` subsetting. For all parameter settings not specified explicitly in the runcard (here, for example, which parton shower or hadronisation model is to be used), their default values are assumed. Accordingly, the given runcard would generate hadron-level events based on SHERPA's Catani–Seymour dipole shower, see Sec. 2.3.1, and its cluster hadronisation model, described in Sec. 2.8.3.

All settings can be specified on the command line, too, using the same syntax, for example:

```
$ Sherpa 'EVENTS: 1M'
```

This would set the number of events to one million, taking precedence over any SHERPA defaults or runcard settings. Some settings have associated command-line arguments, e.g. the following command is an equivalent way to request the generation of one million events:

```
$ Sherpa -e 1M
```

Other arguments on the command line are interpreted as paths to runcards to be used, e.g.

```
$ Sherpa -e 1M path/to/runcard.yaml
```

will read in settings from `path/to/runcard.yaml`, and proceed to generate one million events for the process(es) defined therein.

Because it is easy to introduce a typo in a setting name, or to use the wrong capitalisation (all setting names and values are case-sensitive), SHERPA will report a short summary of any unused settings in the output produced at the end of a run. Additionally, details of all settings, used or unused, and the associated defaults and custom values, are written to the `Settings_Report` directory within the current working directory, which can be understood as a manifest of the run configuration.

For more details on the syntax, a complete documentation of all user settings, available command-line arguments and the settings report, we refer the reader to the manual available on the SHERPA webpage or distributed with the code.

C Details on beam remnant handling

In SHERPA, the breakup of incoming hadrons and the formation of the beam remnants is modelled after all multiple-parton interactions and associated parton showering steps have terminated and a list of shower initiators can be extracted from the incoming hadron. The physics model is the following:

1. Flavour compensation: assuming an incoming hadron to consist of a valence quark–diquark pair (the diquark is the carrier of the baryon number), and that di-quarks cannot act as shower initiators, the flavours of the shower initiators have to be compensated. One of them may be a valence quark – shower initiators are assigned as valence quarks with a probability obtained from the PDFs at the lowest scale. All other "net" quark flavours among the shower initiators are compensated with a corresponding anti-flavour spectator.

2. Colour compensation: as the overall hadron must form a singlet, SHERPA assumes a colour-ordered list of partons of the type $q - g - g - \cdots - (qq)$, where q and (qq) denote the valence quark and diquark. The model also assumes that flavour–anti-flavour pairs, either formed by the shower initiators of independent MPI scatters or by compensating individual flavours with a corresponding anti-flavour spectator, emerge from a gluon and therefore will be in a relative colour-octet state.

3. Longitudinal momenta: The longitudinal momenta of the shower initiators are already fixed, and those for the spectators in the beam breakup are selected according to the PDFs. The longitudinal momentum for the valence diquark is given by the residual at the end of the process.

4. Transverse momentum: SHERPA models the finite "intrinsic" transverse momentum $k_\perp$ inside the hadrons, akin to Fermi motion by assuming a Gaussian distribution, cut-off at large values through a polynomial,

$$\mathcal{P}(k_\perp) \propto \exp(-(k_\perp - k_{\perp,0})^2/\sigma^2)(k_{\perp,\max} - k_\perp)^\eta \,. \tag{C.1}$$

   The parameters of this distribution depend on the hadron forming the beam and scale with the centre-of-mass energy of the collision. SHERPA allows different parameter values for parton-shower initiators and the spectator.

5. Overall momentum conservation: To ensure overall momentum conservation after assigning individual intrinsic transverse momenta for the partons, SHERPA allows two recoil strategies, which slightly modify both transverse and longitudinal momenta. In a "democratic approach" the overall excess transverse momentum is compensated by subtracting it from the partons in proportion to their longitudinal momenta. Alternatively, SHERPA compensates in a similar fashion, the recoil of the shower initiators with the spectators and vice versa. This leaves the question of overall momentum conservation within the beam break-up, as in most cases the combined invariant mass of partons coming from a hadron differs from its mass. In hadron–hadron collisions this is achieved by shuffling momenta between the two hadrons, while in collisions involving only one incident hadron, this compensation happens between the initial state and strongly-interacting final states.

References

[1] A. Buckley et al., *General-purpose event generators for LHC physics*, Phys. Rept. **504** (2011), 145–233, [arXiv:1101.2599 [hep-ph]].

[2] J. M. Campbell et al., *Event generators for high-energy physics experiments*, SciPost Phys. **16** (2024), no. 5, 130, [arXiv:2203.11110 [hep-ph]].

[3] J. Bellm et al., *Herwig 7.0/Herwig++ 3.0 release note*, Eur. Phys. J. **C76** (2016), no. 4, 196, [arXiv:1512.01178 [hep-ph]].

[4] G. Bewick et al., *Herwig 7.3 Release Note*, arXiv:2312.05175 [hep-ph].

[5] T. Sjöstrand, S. Ask, J. R. Christiansen, R. Corke, N. Desai, P. Ilten, S. Mrenna, S. Prestel, C. O. Rasmussen and P. Z. Skands, *An Introduction to PYTHIA 8.2*, Comput. Phys. Commun. **191** (2015), 159–177, [arXiv:1410.3012 [hep-ph]].

[6] C. Bierlich et al., *A comprehensive guide to the physics and usage of PYTHIA 8.3*, SciPost Phys. Codeb. **2022** (2022), 8, [arXiv:2203.11601 [hep-ph]].

[7] R. K. Ellis et al., *Physics Briefing Book: Input for the European Strategy for Particle Physics Update 2020*, arXiv:1910.11775 [hep-ex].

[8] J. N. Butler et al., *Report of the 2021 U.S. Community Study on the Future of Particle Physics (Snowmass 2021)*.

[9] T. Gleisberg, S. Höche, F. Krauss, A. Schälicke, S. Schumann and J. Winter, *SHERPA 1.α, a proof-of-concept version*, JHEP **02** (2004), 056, [hep-ph/0311263].

[10] T. Gleisberg, S. Höche, F. Krauss, M. Schönherr, S. Schumann, F. Siegert and J. Winter, *Event generation with SHERPA 1.1*, JHEP **02** (2009), 007, [arXiv:0811.4622 [hep-ph]].

[11] E. Bothmann et al., *Event Generation with Sherpa 2.2*, SciPost Phys. **7** (2019), no. 3, 034, [arXiv:1905.09127 [hep-ph]].

[12] C. von Weizsäcker, *Radiation emitted in collisions of very fast electrons*, Z.Phys. **88** (1934), 612–625.

[13] E. Williams, *Nature of the high-energy particles of penetrating radiation and status of ionization and radiation formulae*, Phys.Rev. **45** (1934), 729–730.

[14] V. M. Budnev, I. F. Ginzburg, G. V. Meledin and V. G. Serbo, *The two photon particle production mechanism. Physical problems. Applications. Equivalent photon approximation*, Phys. Rept. **15** (1974), 181–281.

[15] S. Frixione, M. L. Mangano, P. Nason and G. Ridolfi, *Improving the Weizsacker-Williams approximation in electron - proton collisions*, Phys. Lett. B **319** (1993), 339–345, [hep-ph/9310350].

[16] J. C. Collins, *Proof of factorization for diffractive hard scattering*, Phys. Rev. D **57** (1998), 3051–3056, [hep-ph/9709499], [Erratum: Phys.Rev.D 61, 019902 (2000)].

[17] G. Ingelman and P. E. Schlein, *Jet Structure in High Mass Diffractive Scattering*, Phys. Lett. B **152** (1985), 256–260.

[18] P. Newman and M. Wing, *The Hadronic Final State at HERA*, Rev. Mod. Phys. **86** (2014), no. 3, 1037, [arXiv:1308.3368 [hep-ex]].

[19] A. Buckley, J. Ferrando, S. Lloyd, K. Nordström, B. Page, M. Rüfenacht, M. Schönherr and G. Watt, *LHAPDF6: parton density access in the LHC precision era*, Eur. Phys. J. **C75** (2015), 132, [arXiv:1412.7420 [hep-ph]].

[20] R. D. Ball et al., PDF4LHC Working Group collaboration, *The PDF4LHC21 combination of global PDF fits for the LHC Run III*, J. Phys. G **49** (2022), no. 8, 080501, [arXiv:2203.05506 [hep-ph]].

[21] R. D. Ball et al., NNPDF collaboration, *Parton distributions from high-precision collider data*, Eur. Phys. J. C **77** (2017), no. 10, 663, [arXiv:1706.00428 [hep-ph]].

[22] S. Dulat, T.-J. Hou, J. Gao, M. Guzzi, J. Huston, P. Nadolsky, J. Pumplin, C. Schmidt, D. Stump and C. P. Yuan, *New parton distribution functions from a global analysis of quantum chromodynamics*, Phys. Rev. **D93** (2016), no. 3, 033006, [arXiv:1506.07443 [hep-ph]].

[23] E. Bothmann, A. Buckley, I. A. Christidi, C. Gütschow, S. Höche, M. Knobbe, T. Martin and M. Schönherr, *Accelerating LHC event generation with simplified pilot runs and fast PDFs*, Eur. Phys. J. C **82** (2022), no. 12, 1128, [arXiv:2209.00843 [hep-ph]].

[24] M. Glück, E. Reya and A. Vogt, *Parton structure of the photon beyond the leading order*, Phys. Rev. **D45** (1992), 3986–3994.

[25] M. Glück, E. Reya and A. Vogt, *Photonic parton distributions*, Phys. Rev. **D46** (1992), 1973–1979.

[26] M. Gluck, E. Reya and I. Schienbein, *Radiatively generated parton distributions of real and virtual photons*, Phys. Rev. D **60** (1999), 054019, [hep-ph/9903337], [Erratum: Phys.Rev.D 62, 019902 (2000)].

[27] W. Slominski, H. Abramowicz and A. Levy, *NLO photon parton parametrization using ee and ep data*, Eur. Phys. J. C **45** (2006), 633–641, [hep-ph/0504003].

[28] F. Cornet, P. Jankowski, M. Krawczyk and A. Lorca, *A New five flavor LO analysis and parametrization of parton distributions in the real photon*, Phys. Rev. D **68** (2003), 014010, [hep-ph/0212160].

[29] F. Cornet, P. Jankowski and M. Krawczyk, *A New 5 flavor NLO analysis and parametrizations of parton distributions of the real photon*, Phys. Rev. D **70** (2004), 093004, [hep-ph/0404063].

[30] G. A. Schuler and T. Sjöstrand, *Low and high mass components of the photon distribution functions*, Z. Phys. C **68** (1995), 607–624, [hep-ph/9503384].

[31] G. A. Schuler and T. Sjöstrand, *Parton distributions of the virtual photon*, Phys.Lett. **B376** (1996), 193–200, [arXiv:hep-ph/9601282 [hep-ph]].

[32] A. Aktas et al., H1 collaboration, *Measurement and QCD analysis of the diffractive deep-inelastic scattering cross-section at HERA*, Eur. Phys. J. C **48** (2006), 715–748, [hep-ex/0606004].

[33] E. A. Kuraev and V. S. Fadin, *On Radiative Corrections to e+ e- Single Photon Annihilation at High-Energy*, Sov. J. Nucl. Phys. **41** (1985), 466–472.

[34] D. Y. Bardin, M. S. Bilenky, A. Olchevski and T. Riemann, *Off-shell W pair production in e+ e- annihilation: Initial state radiation*, Phys. Lett. B **308** (1993), 403–410, [hep-ph/9507277], [Erratum: Phys.Lett.B 357, 725–726 (1995)].

[35] W. Beenakker and A. Denner, *Standard model predictions for W pair production in electron - positron collisions*, Int. J. Mod. Phys. A **9** (1994), 4837–4920.

[36] G. Montagna, O. Nicrosini, G. Passarino and F. Piccinini, *Semianalytical and Monte Carlo results for the production of four fermions in e+ e- collisions*, Phys. Lett. B **348** (1995), 178–184, [hep-ph/9411332].

[37] F. A. Berends, R. Pittau and R. Kleiss, *All electroweak four-fermion processes in electron-positron collisions*, Nucl. Phys. **B424** (1994), 308, [hep-ph/9404313].

[38] F. Krauss, A. Price and M. Schönherr, *YFS Resummation for Future Lepton-Lepton Colliders in SHERPA*, SciPost Phys. **13** (2022), no. 2, 026, [arXiv:2203.10948 [hep-ph]].

[39] F. Krauss, R. Kuhn and G. Soff, *AMEGIC++ 1.0: A Matrix Element Generator In C++*, JHEP **02** (2002), 044, [hep-ph/0109036].

[40] T. Gleisberg and S. Höche, *Comix, a new matrix element generator*, JHEP **12** (2008), 039, [arXiv:0808.3674 [hep-ph]].

[41] J. R. Ellis, M. K. Gaillard and D. V. Nanopoulos, *A Phenomenological Profile of the Higgs Boson*, Nucl.Phys. **B106** (1976), 292.

[42] F. Wilczek, *Decays of Heavy Vector Mesons Into Higgs Particles*, Phys.Rev.Lett. **39** (1977), 1304.

[43] M. A. Shifman, A. Vainshtein, M. Voloshin and V. I. Zakharov, *Low-Energy Theorems for Higgs Boson Couplings to Photons*, Sov.J.Nucl.Phys. **30** (1979), 711–716.

[44] J. R. Ellis, M. Gaillard, D. V. Nanopoulos and C. T. Sachrajda, *Is the Mass of the Higgs Boson About 10-GeV?*, Phys.Lett. **B83** (1979), 339.

[45] C. Degrande, C. Duhr, B. Fuks, D. Grellscheid, O. Mattelaer and T. Reiter, *UFO - The Universal FeynRules Output*, Comput.Phys.Commun. **183** (2012), 1201–1214, [arXiv:1108.2040 [hep-ph]].

[46] L. Darmé et al., *UFO 2.0: the 'Universal Feynman Output' format*, Eur. Phys. J. C **83** (2023), no. 7, 631, [arXiv:2304.09883 [hep-ph]].

[47] E. Byckling and K. Kajantie, *N-particle phase space in terms of invariant momentum transfers*, Nucl. Phys. **B9** (1969), 568–576.

[48] R. Kleiss and R. Pittau, *Weight optimization in multichannel Monte Carlo*, Comput. Phys. Commun. **83** (1994), 141–146, [arXiv:hep-ph/9405257 [hep-ph]].

[49] F. A. Berends, R. Pittau and R. Kleiss, *Excalibur: A Monte Carlo program to evaluate all four fermion processes at LEP-200 and beyond*, Comput. Phys. Commun. **85** (1995), 437–452, [hep-ph/9409326].

[50] G. P. Lepage, *A New Algorithm for Adaptive Multidimensional Integration*, J. Comput. Phys. **27** (1978), 192.

[51] T. Ohl, *Vegas revisited: Adaptive Monte Carlo integration beyond factorization*, Comput. Phys. Commun. **120** (1999), 13–19, [hep-ph/9806432].

[52] F. Cascioli, S. Höche, F. Krauss, P. Maierhöfer, S. Pozzorini and F. Siegert, *Precise Higgs-background predictions: merging NLO QCD and squared quark-loop corrections to four-lepton + 0,1 jet production*, JHEP **01** (2014), 046, [arXiv:1309.0500 [hep-ph]].

[53] D. Goncalves, F. Krauss, S. Kuttimalai and P. Maierhöfer, *Higgs-Strahlung: Merging the NLO Drell-Yan and Loop-Induced 0+1 jet Multiplicities*, Phys. Rev. **D92** (2015), no. 7, 073006, [arXiv:1509.01597 [hep-ph]].

[54] S. Jones and S. Kuttimalai, *Parton Shower and NLO-Matching uncertainties in Higgs Boson Pair Production*, JHEP **02** (2018), 176, [arXiv:1711.03319 [hep-ph]].

[55] E. Bothmann, D. Napoletano, M. Schönherr, S. Schumann and S. L. Villani, *Higher-order EW corrections in ZZ and ZZj production at the LHC*, JHEP **06** (2022), 064, [arXiv:2111.13453 [hep-ph]].

[56] S. Frixione, Z. Kunszt and A. Signer, *Three-jet cross-sections to next-to-leading order*, Nucl. Phys. **B467** (1996), 399–442, [hep-ph/9512328].

[57] S. Catani and M. H. Seymour, *A general algorithm for calculating jet cross sections in NLO QCD*, Nucl. Phys. **B485** (1997), 291–419, [hep-ph/9605323].

[58] S. Catani, S. Dittmaier, M. H. Seymour and Z. Trocsanyi, *The dipole formalism for next-to-leading order QCD calculations with massive partons*, Nucl. Phys. **B627** (2002), 189–265, [hep-ph/0201036].

[59] T. Gleisberg and F. Krauss, *Automating dipole subtraction for QCD NLO calculations*, Eur. Phys. J. **C53** (2008), 501–523, [arXiv:0709.2881 [hep-ph]].

[60] M. Schönherr, *An automated subtraction of NLO EW infrared divergences*, Eur. Phys. J. **C78** (2018), no. 2, 119, [arXiv:1712.07975 [hep-ph]].

[61] S. Kallweit, J. M. Lindert, S. Pozzorini and M. Schönherr, *NLO QCD+EW predictions for $2\ell 2\nu$ diboson signatures at the LHC*, JHEP **11** (2017), 120, [arXiv:1705.00598 [hep-ph]].

[62] M. Chiesa, N. Greiner, M. Schönherr and F. Tramontano, *Electroweak corrections to diphoton plus jets*, JHEP **10** (2017), 181, [arXiv:1706.09022 [hep-ph]].

[63] N. Greiner and M. Schönherr, *NLO QCD+EW corrections to diphoton production in association with a vector boson*, JHEP **01** (2018), 079, [arXiv:1710.11514 [hep-ph]].

[64] M. Reyer, M. Schönherr and S. Schumann, *Full NLO corrections to 3-jet production and R_{32} at the LHC*, Eur. Phys. J. **C79** (2019), no. 4, 321, [arXiv:1902.01763 [hep-ph]].

[65] F. Cascioli, P. Maierhöfer and S. Pozzorini, *Scattering Amplitudes with Open Loops*, Phys.Rev.Lett. **108** (2012), 111601, [arXiv:1111.5206 [hep-ph]].

[66] F. Buccioni, J.-N. Lang, J. M. Lindert, P. Maierhöfer, S. Pozzorini, H. Zhang and M. F. Zoller, *OpenLoops 2*, Eur. Phys. J. C **79** (2019), no. 10, 866, [arXiv:1907.13071 [hep-ph]].

[67] S. Actis, A. Denner, L. Hofer, A. Scharf and S. Uccirati, *Recursive generation of one-loop amplitudes in the Standard Model*, JHEP **1304** (2013), 037, [arXiv:1211.6316 [hep-ph]].

[68] A. Denner, J.-N. Lang and S. Uccirati, *Recola2: REcursive Computation of One-Loop Amplitudes 2*, Comput. Phys. Commun. **224** (2018), 346–361, [arXiv:1711.07388 [hep-ph]].

[69] B. Biedermann, S. Bräuer, A. Denner, M. Pellen, S. Schumann and J. M. Thompson, *Automation of NLO QCD and EW corrections with Sherpa and Recola*, Eur. Phys. J. **C77** (2017), 492, [arXiv:1704.05783 [hep-ph]].

[70] V. Hirschi, R. Frederix, S. Frixione, M. V. Garzelli, F. Maltoni and R. Pittau, *Automation of one-loop QCD corrections*, JHEP **05** (2011), 044, [arXiv:1103.0621 [hep-ph]].

[71] J. M. Campbell, S. Höche and C. T. Preuss, *Accelerating LHC phenomenology with analytic one-loop amplitudes: A C++ interface to MCFM*, Eur. Phys. J. C **81** (2021), no. 12, 1117, [arXiv:2107.04472 [hep-ph]].

[72] S. Höche, Y. Li and S. Prestel, *Drell-Yan lepton pair production at NNLO QCD with parton showers*, Phys. Rev. D **91** (2015), no. 7, 074015, [arXiv:1405.3607 [hep-ph]].

[73] S. Höche, Y. Li and S. Prestel, *Higgs-boson production through gluon fusion at NNLO QCD with parton showers*, Phys.Rev. **D90** (2014), 054011, [arXiv:1407.3773 [hep-ph]].

[74] S. Höche, S. Kuttimalai and Y. Li, *Hadronic Final States in DIS at NNLO QCD with Parton Showers*, Phys. Rev. **D98** (2018), no. 11, 114013, [arXiv:1809.04192 [hep-ph]].

[75] S. Catani and M. Grazzini, *An NNLO subtraction formalism in hadron collisions and its application to Higgs boson production at the LHC*, Phys.Rev.Lett. **98** (2007), 222002, [arXiv:hep-ph/0703012 [hep-ph]].

[76] S. Catani, L. Cieri, G. Ferrera, D. de Florian and M. Grazzini, *Vector boson production at hadron colliders: a fully exclusive QCD calculation at NNLO*, Phys.Rev.Lett. **103** (2009), 082001, [arXiv:0903.2120 [hep-ph]].

[77] M. Cacciari, F. A. Dreyer, A. Karlberg, G. P. Salam and G. Zanderighi, *Fully Differential Vector-Boson-Fusion Higgs Production at Next-to-Next-to-Leading Order*, Phys. Rev. Lett. **115** (2015), no. 8, 082002, [arXiv:1506.02660 [hep-ph]], [Erratum: Phys. Rev. Lett.120,no.13,139901(2018)].

[78] S. Höche, S. Kuttimalai, S. Schumann and F. Siegert, *Beyond Standard Model calculations with Sherpa*, Eur. Phys. J. **C75** (2015), no. 3, 135, [arXiv:1412.6478 [hep-ph]].

[79] J. C. Collins, *Spin correlations in Monte Carlo event generators*, Nucl.Phys. **B304** (1988), 794.

[80] I. Knowles, *Angular Correlations in QCD*, Nucl.Phys. **B304** (1988), 767.

[81] I. Knowles, *Spin Correlations in Parton - Parton Scattering*, Nucl.Phys. **B310** (1988), 571.

[82] P. Richardson, *Spin correlations in Monte Carlo simulations*, JHEP **11** (2001), 029, [hep-ph/0110108].

[83] ILC collaboration, *The International Linear Collider Technical Design Report - Volume 2: Physics*, arXiv:1306.6352 [hep-ph].

[84] T. K. Charles et al., CLICdp, CLIC collaboration, *The Compact Linear Collider (CLIC) - 2018 Summary Report*, arXiv:1812.06018 [physics.acc-ph].

[85] G. Moortgat-Pick et al., *The Role of polarized positrons and electrons in revealing fundamental interactions at the linear collider*, Phys. Rept. **460** (2008), 131–243, [hep-ph/0507011].

[86] W. Kilian, T. Ohl and J. Reuter, *WHIZARD: Simulating Multi-Particle Processes at LHC and ILC*, Eur. Phys. J. **C71** (2007), 1742, [arXiv:0708.4233 [hep-ph]].

[87] J. Alwall, R. Frederix, S. Frixione, V. Hirschi, F. Maltoni, O. Mattelaer, H.-S. Shao, T. Stelzer, P. Torrielli and M. Zaro, *The automated computation of tree-level and next-to-leading order differential cross sections, and their matching to parton shower simulations*, JHEP **07** (2014), 079, [arXiv:1405.0301 [hep-ph]].

[88] M. Hoppe, M. Schönherr and F. Siegert, *Polarised cross sections for vector boson production with Sherpa*, JHEP **04** (2024), 001, [arXiv:2310.14803 [hep-ph]].

[89] E. Bothmann et al., *A standard convention for particle-level Monte Carlo event-variation weights*, SciPost Phys. Core **6** (2023), 007, [arXiv:2203.08230 [hep-ph]].

[90] A. Denner and G. Pelliccioli, *NLO QCD predictions for doubly-polarized WZ production at the LHC*, Phys. Lett. B **814** (2021), 136107, [arXiv:2010.07149 [hep-ph]].

[91] V. A. Kuzmin, V. A. Rubakov and M. E. Shaposhnikov, *On the Anomalous Electroweak Baryon Number Nonconservation in the Early Universe*, Phys. Lett. B **155** (1985), 36.

[92] M. Fukugita and T. Yanagida, *Baryogenesis Without Grand Unification*, Phys. Lett. B **174** (1986), 45–47.

[93] G. 't Hooft, *Symmetry Breaking Through Bell-Jackiw Anomalies*, Phys. Rev. Lett. **37** (1976), 8–11.

[94] V. V. Khoze, F. Krauss and M. Schott, *Large Effects from Small QCD Instantons: Making Soft Bombs at Hadron Colliders*, JHEP **04** (2020), 201, [arXiv:1911.09726 [hep-ph]].

[95] N. D. Christensen, P. de Aquino, C. Degrande, C. Duhr, B. Fuks, M. Herquet, F. Maltoni and S. Schumann, *A comprehensive approach to new physics simulations*, Eur. Phys. J. **C71** (2011), 1541, [arXiv:0906.2474 [hep-ph]].

[96] S. P. Martin, *A Supersymmetry primer*, Adv. Ser. Direct. High Energy Phys. **18** (1998), 1–98, [hep-ph/9709356].

[97] P. Skands et al., *SUSY Les Houches accord: interfacing SUSY spectrum calculators, decay packages, and event generators*, JHEP **07** (2004), 036, [hep-ph/0311123].

[98] K. Hagiwara, R. D. Peccei, D. Zeppenfeld and K. Hikasa, *Probing the weak boson sector in $e^+e^- \to W^+W^-$*, Nucl. Phys. **B282** (1987), 253.

[99] A. Belyaev, O. J. Eboli, M. Gonzalez-Garcia, J. Mizukoshi, S. Novaes and I. Zacharov, *Strongly interacting vector bosons at the CERN LHC: Quartic anomalous couplings*, Phys.Rev. **D59** (1999), 015022, [arXiv:hep-ph/9805229 [hep-ph]].

[100] O. J. Eboli, M. Gonzalez-Garcia, S. Lietti and S. Novaes, *Anomalous quartic gauge boson couplings at hadron colliders*, Phys.Rev. **D63** (2001), 075008, [arXiv:hep-ph/0009262 [hep-ph]].

[101] O. Eboli, M. Gonzalez-Garcia and S. Lietti, *Bosonic quartic couplings at CERN LHC*, Phys.Rev. **D69** (2004), 095005, [arXiv:hep-ph/0310141 [hep-ph]].

[102] O. Eboli, M. Gonzalez-Garcia and J. Mizukoshi, *$pp \to jje^\pm\mu^\pm\nu\nu$ and $jje^\pm\mu^\mp\nu\nu$ at $O(\alpha_{em}^6)$ and $O(\alpha_{em}^4\alpha_s^2)$ for the study of the quartic electroweak gauge boson vertex at CERN LHC*, Phys.Rev. **D74** (2006), 073005, [hep-ph/0606118].

[103] A. Biekötter, R. Gomez-Ambrosio, P. Gregg, F. Krauss and M. Schönherr, *Constraining SMEFT operators with associated $h\gamma$ production in weak boson fusion*, Phys. Lett. B **814** (2021), 136079, [arXiv:2003.06379 [hep-ph]].

[104] A. Biekötter, P. Gregg, F. Krauss and M. Schönherr, *Constraining CP violating operators in charged and neutral triple gauge couplings*, Phys. Lett. B **817** (2021), 136311, [arXiv:2102.01115 [hep-ph]].

[105] S. Banerjee, D. Reichelt and M. Spannowsky, *Electroweak Corrections and EFT Operators in W^+W^- production at the LHC*, arXiv:2406.15640 [hep-ph].

[106] N. D. Christensen, P. de Aquino, N. Deutschmann, C. Duhr, B. Fuks, C. Garcia-Cely, O. Mattelaer, K. Mawatari, B. Oexl and Y. Takaesu, *Simulating spin-$\frac{3}{2}$ particles at colliders*, Eur. Phys. J. C **73** (2013), no. 10, 2580, [arXiv:1308.1668 [hep-ph]].

[107] J. Alwall, C. Duhr, B. Fuks, O. Mattelaer, D. G. Öztürk and C.-H. Shen, *Computing decay rates for new physics theories with FeynRules and MadGraph 5_aMC@NLO*, Comput. Phys. Commun. **197** (2015), 312–323, [arXiv:1402.1178 [hep-ph]].

[108] R. Aoude, F. Maltoni, O. Mattelaer, C. Severi and E. Vryonidou, *Renormalisation group effects on SMEFT interpretations of LHC data*, JHEP **09** (2023), 191, [arXiv:2212.05067 [hep-ph]].

[109] B. R. Webber, *A QCD model for jet fragmentation including soft gluon interference*, Nucl. Phys. **B238** (1984), 492.

[110] M. Bengtsson, T. Sjöstrand and M. van Zijl, *Initial State Radiation Effects on W and Jet Production*, Z. Phys. **C32** (1986), 67.

[111] M. Bengtsson and T. Sjöstrand, *A comparative study of coherent and non-coherent parton shower evolution*, Nucl. Phys. **B289** (1987), 810.

[112] G. Marchesini and B. R. Webber, *Monte Carlo Simulation of General Hard Processes with Coherent QCD Radiation*, Nucl. Phys. **B310** (1988), 461.

[113] G. Gustafson and U. Pettersson, *Dipole formulation of QCD cascades*, Nucl. Phys. **B306** (1988), 746.

[114] B. Andersson, G. Gustafson and L. Lönnblad, *Gluon splitting in the color dipole cascades*, Nucl. Phys. **B339** (1990), 393–406.

[115] L. Lönnblad, *Ariadne version 4: A program for simulation of QCD cascades implementing the colour dipole model*, Comput. Phys. Commun. **71** (1992), 15–31.

[116] S. Schumann and F. Krauss, *A parton shower algorithm based on Catani-Seymour dipole factorisation*, JHEP **03** (2008), 038, [arXiv:0709.1027 [hep-ph]].

[117] Z. Nagy and D. E. Soper, *A new parton shower algorithm: Shower evolution, matching at leading and next-to-leading order level*, hep-ph/0601021.

[118] S. Höche, F. Krauss and M. Schönherr, *Uncertainties in MEPS@NLO calculations of h+jets*, Phys. Rev. **D90** (2014), no. 1, 014012, [arXiv:1401.7971 [hep-ph]].

[119] F. Krauss, D. Napoletano and S. Schumann, *Simulating b-associated production of Z and Higgs bosons with the SHERPA event generator*, Phys. Rev. **D95** (2017), no. 3, 036012, [arXiv:1612.04640 [hep-ph]].

[120] F. Krauss and D. Napoletano, *Towards a fully massive five-flavor scheme*, Phys. Rev. **D98** (2018), no. 9, 096002, [arXiv:1712.06832 [hep-ph]].

[121] S. Höche, S. Schumann and F. Siegert, *Hard photon production and matrix-element parton-shower merging*, Phys. Rev. **D81** (2010), 034026, [arXiv:0912.3501 [hep-ph]].

[122] S. Höche and S. Prestel, *The midpoint between dipole and parton showers*, Eur. Phys. J. **C75** (2015), no. 9, 461, [arXiv:1506.05057 [hep-ph]].

[123] S. Höche and S. Prestel, *Triple collinear emissions in parton showers*, Phys. Rev. **D96** (2017), no. 7, 074017, [arXiv:1705.00742 [hep-ph]].

[124] F. Dulat, S. Höche and S. Prestel, *Leading-Color Fully Differential Two-Loop Soft Corrections to QCD Dipole Showers*, Phys. Rev. **D98** (2018), no. 7, 074013, [arXiv:1805.03757 [hep-ph]].

[125] L. Gellersen, S. Höche and S. Prestel, *Disentangling soft and collinear effects in QCD parton showers*, Phys. Rev. D **105** (2022), no. 11, 114012, [arXiv:2110.05964 [hep-ph]].

[126] M. Dasgupta, F. A. Dreyer, K. Hamilton, P. F. Monni and G. P. Salam, *Logarithmic accuracy of parton showers: a fixed-order study*, JHEP **09** (2018), 033, [arXiv:1805.09327 [hep-ph]].

[127] F. Herren, S. Höche, F. Krauss, D. Reichelt and M. Schönherr, *A new approach to color-coherent parton evolution*, JHEP **10** (2023), 091, [arXiv:2208.06057 [hep-ph]].

[128] M. Dasgupta, F. A. Dreyer, K. Hamilton, P. F. Monni, G. P. Salam and G. Soyez, *Parton showers beyond leading logarithmic accuracy*, Phys. Rev. Lett. **125** (2020), no. 5, 052002, [arXiv:2002.11114 [hep-ph]].

[129] B. Assi and S. Höche, *New approach to QCD final-state evolution in processes with massive partons*, Phys. Rev. D **109** (2024), no. 11, 114008, [arXiv:2307.00728 [hep-ph]].

[130] S. Höche, F. Krauss and D. Reichelt, *The Alaric parton shower for hadron colliders*, arXiv:2404.14360 [hep-ph].

[131] S. Höche, D. Reichelt and F. Siegert, *Momentum conservation and unitarity in parton showers and NLL resummation*, JHEP **01** (2018), 118, [arXiv:1711.03497 [hep-ph]].

[132] G. Aad et al., ATLAS collaboration, *ATLAS Measurements of the Properties of Jets for Boosted Particle Searches*, Phys. Rev. D **86** (2012), 072006, [arXiv:1206.5369 [hep-ex]].

[133] S. Frixione and B. R. Webber, *Matching NLO QCD computations and parton shower simulations*, JHEP **06** (2002), 029, [hep-ph/0204244].

[134] P. Nason, *A new method for combining NLO QCD with shower Monte Carlo algorithms*, JHEP **11** (2004), 040, [hep-ph/0409146].

[135] S. Frixione, P. Nason and C. Oleari, *Matching NLO QCD computations with parton shower simulations: the POWHEG method*, JHEP **11** (2007), 070, [arXiv:0709.2092 [hep-ph]].

[136] S. Jadach, W. Płaczek, S. Sapeta, A. Siódmok and M. Skrzypek, *Matching NLO QCD with parton shower in Monte Carlo scheme — the KrkNLO method*, JHEP **10** (2015), 052, [arXiv:1503.06849 [hep-ph]].

[137] L. Lönnblad and S. Prestel, *Merging Multi-leg NLO Matrix Elements with Parton Showers*, JHEP **03** (2013), 166, [arXiv:1211.7278 [hep-ph]].

[138] P. Nason and G. P. Salam, *Multiplicative-accumulative matching of NLO calculations with parton showers*, JHEP **01** (2022), 067, [arXiv:2111.03553 [hep-ph]].

[139] S. Höche, F. Krauss, M. Schönherr and F. Siegert, *A critical appraisal of NLO+PS matching methods*, JHEP **09** (2012), 049, [arXiv:1111.1220 [hep-ph]].

[140] S. Höche and M. Schönherr, *Uncertainties in next-to-leading order plus parton shower matched simulations of inclusive jet and dijet production*, Phys.Rev. **D86** (2012), 094042, [arXiv:1208.2815 [hep-ph]].

[141] S. Höche, J. Huang, G. Luisoni, M. Schönherr and J. Winter, *Zero and one jet combined NLO analysis of the top quark forward-backward asymmetry*, Phys.Rev. **D88** (2013), 014040, [arXiv:1306.2703 [hep-ph]].

[142] J. Bellm et al., *Jet Cross Sections at the LHC and the Quest for Higher Precision*, Eur. Phys. J. C **80** (2020), no. 2, 93, [arXiv:1903.12563 [hep-ph]].

[143] A. Buckley et al., *A comparative study of Higgs boson production from vector-boson fusion*, JHEP **11** (2021), 108, [arXiv:2105.11399 [hep-ph]].

[144] S. Höche, F. Krauss, M. Schönherr and F. Siegert, *W+ n-Jet predictions at the Large Hadron Collider at next-to-leading order matched with a parton shower*, Phys. Rev. Lett. **110** (2013), no. 5, 052001, [arXiv:1201.5882 [hep-ph]].

[145] J. R. Andersen et al., *Les Houches 2015: Physics at TeV Colliders Standard Model Working Group Report*, 9th Les Houches Workshop on Physics at TeV Colliders, 5 2016.

[146] M. Aaboud et al., ATLAS collaboration, *Measurements of Higgs boson properties in the diphoton decay channel with 36 fb^{-1} of pp collision data at $\sqrt{s} = 13$ TeV with the ATLAS detector*, Phys. Rev. D **98** (2018), 052005, [arXiv:1802.04146 [hep-ex]].

[147] K. Danziger, S. Höche and F. Siegert, *Reducing negative weights in Monte Carlo event generation with Sherpa*, arXiv:2110.15211 [hep-ph].

[148] P. Achard et al., L3 collaboration, *Inclusive jet production in two-photon collisions at LEP*, Phys. Lett. B **602** (2004), 157–166, [hep-ex/0410012].

[149] K. Ackerstaff et al., OPAL collaboration, *Inclusive jet production in photon-photon collisions at $\sqrt{s}$ = 130-GeV and 136-GeV*, Z. Phys. C **73** (1997), 433–442.

[150] G. Abbiendi et al., OPAL collaboration, *Inclusive Jet Production in Photon-Photon Collisions at s(ee)**(1/2) from 189 to 209-GeV*, Phys. Lett. B **658** (2008), 185–192, [arXiv:0706.4382 [hep-ex]].

[151] J. Breitweg et al., ZEUS collaboration, *Dijet cross-sections in photoproduction at HERA*, Eur. Phys. J. C **1** (1998), 109–122, [hep-ex/9710018].

[152] H. Abramowicz et al., ZEUS collaboration, *Inclusive-jet photoproduction at HERA and determination of alphas*, Nucl. Phys. B **864** (2012), 1–37, [arXiv:1205.6153 [hep-ex]].

[153] A. Aktas et al., H1 collaboration, *Photoproduction of dijets with high transverse momenta at HERA*, Phys. Lett. B **639** (2006), 21–31, [hep-ex/0603014].

[154] M. Aaboud et al., ATLAS collaboration, *Evidence for light-by-light scattering in heavy-ion collisions with the ATLAS detector at the LHC*, Nature Phys. **13** (2017), no. 9, 852–858, [arXiv:1702.01625 [hep-ex]].

[155] J. Adams et al., STAR collaboration, *Production of e+ e- pairs accompanied by nuclear dissociation in ultra-peripheral heavy ion collision*, Phys. Rev. C **70** (2004), 031902, [nucl-ex/0404012].

[156] J. Adam et al., STAR collaboration, *Measurement of e^+e^- Momentum and Angular Distributions from Linearly Polarized Photon Collisions*, Phys. Rev. Lett. **127** (2021), no. 5, 052302, [arXiv:1910.12400 [nucl-ex]].

[157] B. I. Abelev et al., STAR collaboration, *Observation of pi+ pi- pi+ pi- Photoproduction in Ultra-Peripheral Heavy Ion Collisions at STAR*, Phys. Rev. C **81** (2010), 044901, [arXiv:0912.0604 [nucl-ex]].

[158] G. A. Schuler and T. Sjöstrand, *A Scenario for high-energy gamma gamma interactions*, Z. Phys. C **73** (1997), 677–688, [hep-ph/9605240].

[159] S. Hoeche, F. Krauss and P. Meinzinger, *Resolved photons in Sherpa*, Eur. Phys. J. C **84** (2024), no. 2, 178, [arXiv:2310.18674 [hep-ph]].

[160] P. Meinzinger and F. Krauss, *Hadron-level NLO predictions for QCD observables in photo-production at the Electron-Ion Collider*, Phys. Rev. D **109** (2024), no. 3, 034037, [arXiv:2311.14571 [hep-ph]].

[161] V. Andreev et al., H1 collaboration, *Diffractive Dijet Production with a Leading Proton in ep Collisions at HERA*, JHEP **05** (2015), 056, [arXiv:1502.01683 [hep-ex]].

[162] R. Abdul Khalek et al., *Science Requirements and Detector Concepts for the Electron-Ion Collider: EIC Yellow Report*, Nucl. Phys. A **1026** (2022), 122447, [arXiv:2103.05419 [physics.ins-det]].

[163] F. Krauss and P. Meinzinger, *Hard diffraction in SHERPA*, Eur. Phys. J. C **84** (2024), no. 9, 894, [arXiv:2407.02133 [hep-ph]].

[164] T. Gehrmann, S. Höche, F. Krauss, M. Schönherr and F. Siegert, *NLO QCD matrix elements + parton showers in e^+e^- →hadrons*, JHEP **01** (2013), 144, [arXiv:1207.5031 [hep-ph]].

[165] N. Baberuxki, C. T. Preuss, D. Reichelt and S. Schumann, *Resummed predictions for jet-resolution scales in multijet production in e^+e^- annihilation*, JHEP **04** (2020), 112, [arXiv:1912.09396 [hep-ph]].

[166] M. Knobbe, D. Reichelt and S. Schumann, *(N)NLO+NLL' accurate predictions for plain and groomed 1-jettiness in neutral current DIS*, JHEP **09** (2023), 194, [arXiv:2306.17736 [hep-ph]].

[167] J. Baron, D. Reichelt, S. Schumann, N. Schwanemann and V. Theeuwes, *Soft-drop grooming for hadronic event shapes*, JHEP **07** (2021), 142, [arXiv:2012.09574 [hep-ph]].

[168] S. Höche, F. Krauss, M. Schönherr and F. Siegert, *QCD matrix elements + parton showers: The NLO case*, JHEP **04** (2013), 027, [arXiv:1207.5030 [hep-ph]].

[169] G. Aad et al., ATLAS collaboration, *Measurement of isolated-photon plus two-jet production in pp collisions at $\sqrt{s} = 13$ TeV with the ATLAS detector*, JHEP **03** (2020), 179, [arXiv:1912.09866 [hep-ex]].

[170] J. M. Lindert, S. Pozzorini and M. Schönherr, *Precise predictions for V + 2 jet backgrounds in searches for invisible Higgs decays*, JHEP **01** (2023), 070, [arXiv:2204.07652 [hep-ph]].

[171] S. Bräuer, A. Denner, M. Pellen, M. Schönherr and S. Schumann, *Fixed-order and merged parton-shower predictions for WW and WWj production at the LHC including NLO QCD and EW corrections*, JHEP **10** (2020), 159, [arXiv:2005.12128 [hep-ph]].

[172] J. Krause and F. Siegert, *NLO QCD predictions for $Z + \gamma$ + jets production with Sherpa*, Eur. Phys. J. **C78** (2018), no. 2, 161, [arXiv:1708.06283 [hep-ph]].

[173] F. Siegert, *A practical guide to event generation for prompt photon production with Sherpa*, J. Phys. **G44** (2017), no. 4, 044007, [arXiv:1611.07226 [hep-ph]].

[174] G. Aad et al., ATLAS collaboration, *Measurement of the production cross section of pairs of isolated photons in pp collisions at 13 TeV with the ATLAS detector*, JHEP **11** (2021), 169, [arXiv:2107.09330 [hep-ex]].

[175] S. Höche, F. Krauss, S. Pozzorini, M. Schönherr, J. Thompson, S. Pozzorini and K. C. Zapp, *Triple vector boson production through Higgs-Strahlung with NLO multijet merging*, Phys.Rev. **D89** (2014), 093015, [arXiv:1403.7516 [hep-ph]].

[176] D. Goncalves, F. Krauss, S. Kuttimalai and P. Maierhöfer, *Boosting invisible searches via ZH : From the Higgs boson to dark matter simplified models*, Phys. Rev. D **94** (2016), no. 5, 053014, [arXiv:1605.08039 [hep-ph]].

[177] A. Denner, M. Pellen, M. Schönherr and S. Schumann, *Tri-boson and WH production in the W^+W^+jj channel: predictions at full NLO accuracy and beyond*, JHEP **08** (2024), 043, [arXiv:2406.11516 [hep-ph]].

[178] G. Aad et al., ATLAS collaboration, *Observation of $WZ\gamma$ Production in pp Collisions at s=13 TeV with the ATLAS Detector*, Phys. Rev. Lett. **132** (2024), no. 2, 021802, [arXiv:2305.16994 [hep-ex]].

[179] G. Aad et al., ATLAS collaboration, *Measurement of $Z\gamma\gamma$ production in pp collisions at $\sqrt{s} = 13$ TeV with the ATLAS detector*, Eur. Phys. J. C **83** (2023), no. 6, 539, [arXiv:2211.14171 [hep-ex]].

[180] G. Aad et al., ATLAS collaboration, *Observation of $W\gamma\gamma$ triboson production in proton-proton collisions at $\sqrt{s} = 13$ TeV with the ATLAS detector*, Phys. Lett. B **848** (2024), 138400, [arXiv:2308.03041 [hep-ex]].

[181] ATLAS collaboration, *Modelling of isolated multi-photon production in Monte Carlo generators in ATLAS*.

[182] E. Bothmann, F. Krauss and M. Schönherr, *Single top-quark production with SHERPA*, Eur. Phys. J. **C78** (2018), no. 3, 220, [arXiv:1711.02568 [hep-ph]].

[183] S. Höche, F. Krauss, P. Maierhöfer, S. Pozzorini, M. Schönherr and F. Siegert, *Next-to-leading order QCD predictions for top-quark pair production with up to two jets merged with a parton shower*, Phys. Lett. **B748** (2015), 74–78, [arXiv:1402.6293 [hep-ph]].

[184] C. Gütschow, J. M. Lindert and M. Schönherr, *Multi-jet merged top-pair production including electroweak corrections*, Eur. Phys. J. **C78** (2018), no. 4, 317, [arXiv:1803.00950 [hep-ph]].

[185] ATLAS collaboration, *Modelling of rare top quark processes at $\sqrt{s}$ = 13 TeV in ATLAS*.

[186] F. Cascioli, P. Maierhöfer, N. Moretti, S. Pozzorini and F. Siegert, *NLO matching for $t\bar{t}b\bar{b}$ production with massive b-quarks*, Phys. Lett. **B734** (2014), 210–214, [arXiv:1309.5912 [hep-ph]].

[187] S. Höche, J. Krause and F. Siegert, *Multijet Merging in a Variable Flavor Number Scheme*, Phys. Rev. D **100** (2019), no. 1, 014011, [arXiv:1904.09382 [hep-ph]].

[188] L. Ferencz, S. Höche, J. Katzy and F. Siegert, *$t\bar{t}b\bar{b}$ at NLO precision in a variable flavor number scheme*, JHEP **07** (2024), 026, [arXiv:2402.15497 [hep-ph]].

[189] S. Höche, F. Krauss, M. Schönherr and F. Siegert, *NLO matrix elements and truncated showers*, JHEP **08** (2011), 123, [arXiv:1009.1127 [hep-ph]].

[190] S. Catani, F. Krauss, R. Kuhn and B. R. Webber, *QCD matrix elements + parton showers*, JHEP **11** (2001), 063, [hep-ph/0109231].

[191] L. Lönnblad, *Correcting the colour-dipole cascade model with fixed order matrix elements*, JHEP **05** (2002), 046, [hep-ph/0112284].

[192] F. Krauss, *Matrix elements and parton showers in hadronic interactions*, JHEP **08** (2002), 015, [hep-ph/0205283].

[193] J. Alwall et al., *Comparative study of various algorithms for the merging of parton showers and matrix elements in hadronic collisions*, Eur. Phys. J. **C53** (2008), 473–500, [arXiv:0706.2569 [hep-ph]].

[194] S. Höche, F. Krauss, S. Schumann and F. Siegert, *QCD matrix elements and truncated showers*, JHEP **05** (2009), 053, [arXiv:0903.1219 [hep-ph]].

[195] L. Lönnblad and S. Prestel, *Matching Tree-Level Matrix Elements with Interleaved Showers*, JHEP **03** (2012), 019, [arXiv:1109.4829 [hep-ph]].

[196] R. Frederix and S. Frixione, *Merging meets matching in MC@NLO*, JHEP **12** (2012), 061, [arXiv:1209.6215 [hep-ph]].

[197] S. Plätzer, *Controlling inclusive cross sections in parton shower + matrix element merging*, JHEP **08** (2013), 114, [arXiv:1211.5467 [hep-ph]].

[198] S. Höche, S. Prestel and H. Schulz, *Simulation of Vector Boson Plus Many Jet Final States at the High Luminosity LHC*, Phys. Rev. D **100** (2019), no. 1, 014024, [arXiv:1905.05120 [hep-ph]].

[199] E. Bothmann, T. Childers, C. Gütschow, S. Höche, P. Hovland, J. Isaacson, M. Knobbe and R. Latham, *Efficient precision simulation of processes with many-jet final states at the LHC*, Phys. Rev. D **109** (2024), no. 1, 014013, [arXiv:2309.13154 [hep-ph]].

[200] S. Höche, S. Mrenna, S. Payne, C. T. Preuss and P. Skands, *A Study of QCD Radiation in VBF Higgs Production with Vincia and Pythia*, SciPost Phys. **12** (2022), no. 1, 010, [arXiv:2106.10987 [hep-ph]].

[201] T. Carli, T. Gehrmann and S. Höche, *Hadronic final states in deep-inelastic scattering with Sherpa*, Eur. Phys. J. **C67** (2010), 73, [arXiv:0912.3715 [hep-ph]].

[202] S. Forte, D. Napoletano and M. Ubiali, *Higgs production in bottom-quark fusion: matching beyond leading order*, Phys. Lett. **B763** (2016), 190–196, [arXiv:1607.00389 [hep-ph]].

[203] A. Denner and S. Rode, *Automated resummation of electroweak Sudakov logarithms in diboson production at future colliders*, Eur. Phys. J. C **84** (2024), no. 5, 542, [arXiv:2402.10503 [hep-ph]].

[204] S. Kallweit, J. M. Lindert, P. Maierhöfer, S. Pozzorini and M. Schönherr, *NLO QCD+EW predictions for V + jets including off-shell vector-boson decays and multijet merging*, JHEP **04** (2016), 021, [arXiv:1511.08692 [hep-ph]].

[205] C. Gütschow and M. Schönherr, *Four lepton production and the accuracy of QED FSR*, Eur. Phys. J. C **81** (2021), no. 1, 48, [arXiv:2007.15360 [hep-ph]].

[206] A. Denner and S. Pozzorini, *One loop leading logarithms in electroweak radiative corrections. 1. Results*, Eur.Phys.J. **C18** (2001), 461–480, [arXiv:hep-ph/0010201 [hep-ph]].

[207] A. Denner and S. Pozzorini, *One loop leading logarithms in electroweak radiative corrections. 2. Factorization of collinear singularities*, Eur.Phys.J. **C21** (2001), 63–79, [arXiv:hep-ph/0104127 [hep-ph]].

[208] E. Bothmann and D. Napoletano, *Automated evaluation of electroweak Sudakov logarithms in Sherpa*, Eur. Phys. J. C **80** (2020), no. 11, 1024, [arXiv:2006.14635 [hep-ph]].

[209] D. Pagani and M. Zaro, *One-loop electroweak Sudakov logarithms: a revisitation and automation*, JHEP **02** (2022), 161, [arXiv:2110.03714 [hep-ph]].

[210] D. Pagani, T. Vitos and M. Zaro, *Improving NLO QCD event generators with high-energy EW corrections*, Eur. Phys. J. C **84** (2024), no. 5, 514, [arXiv:2309.00452 [hep-ph]].

[211] J. M. Lindert and L. Mai, *Logarithmic EW corrections at one-loop*, arXiv:2312.07927 [hep-ph].

[212] D. R. Yennie, S. C. Frautschi and H. Suura, *The Infrared Divergence Phenomena and High-Energy Processes*, Ann. Phys. **13** (1961), 379–452.

[213] M. Schönherr and F. Krauss, *Soft photon radiation in particle decays in SHERPA*, JHEP **12** (2008), 018, [arXiv:0810.5071 [hep-ph]].

[214] S. Alioli et al., *Precision studies of observables in $pp \to W \to l\nu_l$ and $pp \to \gamma, Z \to l^+l^-$ processes at the LHC*, Eur. Phys. J. **C77** (2017), no. 5, 280, [arXiv:1606.02330 [hep-ph]].

[215] F. U. Bernlochner and M. Schönherr, *Comparing different ansatzes to describe electroweak radiative corrections to exclusive semileptonic B meson decays into (pseudo)scalar final state mesons using Monte-Carlo techniques*, arXiv:1010.5997 [hep-ph].

[216] F. Krauss, J. M. Lindert, R. Linten and M. Schönherr, *Accurate simulation of W, Z and Higgs boson decays in Sherpa*, Eur. Phys. J. **C79** (2019), no. 2, 143, [arXiv:1809.10650 [hep-ph]].

[217] L. Flower and M. Schönherr, *Photon splitting corrections to soft-photon resummation*, JHEP **03** (2023), 238, [arXiv:2210.07007 [hep-ph]].

[218] G. Altarelli and G. Parisi, *Asymptotic freedom in parton language*, Nucl. Phys. **B126** (1977), 298–318.

[219] V. N. Gribov and L. N. Lipatov, *Deep inelastic e-p scattering in perturbation theory*, Sov. J. Nucl. Phys. **15** (1972), 438–450.

[220] L. N. Lipatov, *The parton model and perturbation theory*, Sov. J. Nucl. Phys. **20** (1975), 94–102.

[221] Y. L. Dokshitzer, *Calculation of the structure functions for deep inelastic scattering and e^+e^- annihilation by perturbation theory in quantum chromodynamics*, Sov. Phys. JETP **46** (1977), 641–653.

[222] M. Skrzypek and S. Jadach, *Exact and approximate solutions for the electron nonsinglet structure function in QED*, Z. Phys. C **49** (1991), 577–584.

[223] S. Jadach, W. Płaczek, M. Skrzypek, B. F. L. Ward and Z. Wąs, *The Monte Carlo program KoralW version 1.51 and the concurrent Monte Carlo KoralW&YFSWW3 with all background graphs and first order corrections to W pair production*, Comput. Phys. Commun. **140** (2001), 475–512, [hep-ph/0104049].

[224] S. Jadach, B. F. L. Ward and Z. Wąs, *The precision Monte Carlo event generator $\mathcal{KK}$ for two- fermion final states in e^+e^- collisions*, Comput. Phys. Commun. **130** (2000), 260–325, [hep-ph/9912214].

[225] S. Jadach, E. Richter-Was, B. F. L. Ward and Z. Was, *Monte Carlo program BHLUMI-2.01 for Bhabha scattering at low angles with Yennie-Frautschi-Suura exponentiation*, Comput. Phys. Commun. **70** (1992), 305–344.

[226] S. Jadach, B. F. L. Ward, Z. Was, S. A. Yost and A. Siodmok, *Multi-photon Monte Carlo event generator KKMCee for lepton and quark pair production in lepton colliders*, Comput. Phys. Commun. **283** (2023), 108556, [arXiv:2204.11949 [hep-ph]].

[227] S. Schael et al., ALEPH, DELPHI, L3, OPAL, SLD, LEP Electroweak Working Group, SLD Electroweak Group, SLD Heavy Flavour Group collaboration, *Precision electroweak measurements on the Z resonance*, Phys. Rept. **427** (2006), 257–454, [hep-ex/0509008].

[228] T. Sjöstrand and M. van Zijl, *A multiple-interaction model for the event structure in hadron collisions*, Phys. Rev. **D36** (1987), 2019.

[229] T. Sjöstrand and P. Z. Skands, *Multiple interactions and the structure of beam remnants*, JHEP **03** (2004), 053, [hep-ph/0402078].

[230] T. Sjöstrand and P. Z. Skands, *Transverse-momentum-ordered showers and interleaved multiple interactions*, Eur. Phys. J. **C39** (2005), 129–154, [hep-ph/0408302].

[231] R. Corke and T. Sjostrand, *Multiparton Interactions and Rescattering*, JHEP **01** (2010), 035, [arXiv:0911.1909 [hep-ph]].

[232] A. De Roeck and H. Jung (Eds.), *HERA and the LHC: A Workshop on the implications of HERA for LHC physics: Proceedings Part A*, Geneva, CERN, CERN, 2005.

[233] A. B. Kaidalov, V. A. Khoze, A. D. Martin and M. G. Ryskin, *Probabilities of rapidity gaps in high-energy interactions*, Eur. Phys. J. C **21** (2001), 521–529, [hep-ph/0105145].

[234] A. B. Kaidalov, V. A. Khoze, A. D. Martin and M. G. Ryskin, *Unitarity effects in hard diffraction at HERA*, Phys. Lett. B **567** (2003), 61–68, [hep-ph/0306134].

[235] A. B. Kaidalov, V. A. Khoze, A. D. Martin and M. G. Ryskin, *Factorization breaking in diffractive dijet photoproduction at HERA*, Eur. Phys. J. C **66** (2010), 373–376, [arXiv:0911.3716 [hep-ph]].

[236] Y. L. Dokshitzer, V. A. Khoze, A. H. Mueller and S. I. Troyan, *Basics of perturbative QCD*, Gif-sur-Yvette, France: Ed. Frontieres, 1991.

[237] P. Z. Skands and D. Wicke, *Non-perturbative QCD effects and the top mass at the Tevatron*, Eur. Phys. J. C **52** (2007), 133–140, [hep-ph/0703081].

[238] T. Sjöstrand and V. A. Khoze, *On Color rearrangement in hadronic W+ W- events*, Z. Phys. C **62** (1994), 281–310, [hep-ph/9310242].

[239] V. A. Khoze and T. Sjöstrand, *Color correlations and multiplicities in top events*, Phys. Lett. B **328** (1994), 466–476, [hep-ph/9403394].

[240] V. A. Khoze and T. Sjöstrand, *QCD interconnection studies at linear colliders*, Eur. Phys. J. direct **2** (2000), no. 1, 1, [hep-ph/9912297].

[241] L. Lönnblad and H. Shah, *A spatially constrained QCD colour reconnection in pp, pA, and AA collisions in the Pythia8/Angantyr model*, Eur. Phys. J. C **83** (2023), no. 7, 575, [arXiv:2303.11747 [hep-ph]], [Erratum: Eur.Phys.J.C 83, 639 (2023)].

[242] B. R. Webber, *Color reconnection and Bose-Einstein effects*, J. Phys. G **24** (1998), 287–296, [hep-ph/9708463].

[243] S. Gieseke, C. Rohr and A. Siodmok, *Colour reconnections in Herwig++*, Eur. Phys. J. C **72** (2012), 2225, [arXiv:1206.0041 [hep-ph]].

[244] S. Gieseke, P. Kirchgaeßer and S. Plätzer, *Baryon production from cluster hadronisation*, Eur. Phys. J. C **78** (2018), no. 2, 99, [arXiv:1710.10906 [hep-ph]].

[245] S. Gieseke, P. Kirchgaeßer, S. Plätzer and A. Siodmok, *Colour Reconnection from Soft Gluon Evolution*, JHEP **11** (2018), 149, [arXiv:1808.06770 [hep-ph]].

[246] J. Bellm, C. B. Duncan, S. Gieseke, M. Myska and A. Siódmok, *Spacetime colour reconnection in Herwig 7*, Eur. Phys. J. C **79** (2019), no. 12, 1003, [arXiv:1909.08850 [hep-ph]].

[247] S. Plätzer, *Colour evolution and infrared physics*, JHEP **07** (2023), 126, [arXiv:2204.06956 [hep-ph]].

[248] J.-C. Winter, F. Krauss and G. Soff, *A modified cluster-hadronisation model*, Eur. Phys. J. **C36** (2004), 381–395, [hep-ph/0311085].

[249] G. S. Chahal and F. Krauss, *Cluster Hadronisation in Sherpa*, SciPost Phys. **13** (2022), no. 2, 019, [arXiv:2203.11385 [hep-ph]].

[250] Y. I. Azimov, Y. L. Dokshitzer, V. A. Khoze and S. Troyan, *Similarity of Parton and Hadron Spectra in QCD Jets*, Z.Phys. **C27** (1985), 65–72.

[251] D. Amati and G. Veneziano, *Preconfinement as a Property of Perturbative QCD*, Phys.Lett. **B83** (1979), 87.

[252] A. Bassetto, M. Ciafaloni and G. Marchesini, *Color Singlet Distributions and Mass Damping in Perturbative QCD*, Phys.Lett. **B83** (1979), 207.

[253] G. Marchesini, L. Trentadue and G. Veneziano, *Space-time Description of Color Screening via Jet Calculus Techniques*, Nucl. Phys. B **181** (1981), 335–346.

[254] R. D. Field and R. P. Feynman, *A parametrization of the properties of quark jets*, Nucl. Phys. **B136** (1978), 1.

[255] P. Hoyer, P. Osland, H. G. Sander, T. F. Walsh and P. M. Zerwas, *Quantum Chromodynamics and Jets in e+ e-*, Nucl. Phys. B **161** (1979), 349–372.

[256] A. Ali, E. Pietarinen, G. Kramer and J. Willrodt, *A QCD Analysis of the High-Energy e+ e- Data from PETRA*, Phys. Lett. B **93** (1980), 155–160.

[257] R. D. Field and S. Wolfram, *A QCD model for e^+e^- annihilation*, Nucl. Phys. **B213** (1983), 65.

[258] G. Corcella et al., *HERWIG 6: an event generator for hadron emission reactions with interfering gluons (including supersymmetric processes)*, JHEP **01** (2001), 010, [hep-ph/0011363].

[259] G. Marchesini and B. R. Webber, *Simulation of QCD Jets Including Soft Gluon Interference*, Nucl. Phys. **B238** (1984), 1.

[260] M. R. Masouminia and P. Richardson, *Hadronization and decay of excited heavy hadrons in Herwig 7*, JHEP **07** (2024), 278, [arXiv:2312.02757 [hep-ph]].

[261] A. H. Hoang, O. L. Jin, S. Plätzer and D. Samitz, *Matching Hadronization and Perturbative Evolution: The Cluster Model in Light of Infrared Shower Cutoff Dependence*, arXiv:2404.09856 [hep-ph].

[262] X. Artru and G. Mennessier, *String model and multiproduction*, Nucl. Phys. **B70** (1974), 93–115.

[263] M. G. Bowler, *e^+e^- production of heavy quarks in the string model*, Z. Phys. **C11** (1981), 169.

[264] B. Andersson, G. Gustafson, G. Ingelman and T. Sjöstrand, *Parton Fragmentation and String Dynamics*, Phys. Rept. **97** (1983), 31–145.

[265] T. D. Gottschalk, *An improved description of hadronization in the QCD cluster model for e^+e^- annihilation*, Nucl. Phys. **B239** (1984), 349.

[266] T. D. Gottschalk and D. A. Morris, *A new model for hadronization and e^+e^- annihilation*, Nucl. Phys. **B288** (1987), 729.

[267] F. Sauter, *Uber das Verhalten eines Elektrons im homogenen elektrischen Feld nach der relativistischen Theorie Diracs*, Z. Phys. **69** (1931), 742–764.

[268] J. S. Schwinger, *On gauge invariance and vacuum polarization*, Phys. Rev. **82** (1951), 664–679.

[269] B. Andersson, G. Gustafson and B. Söderberg, *A general model for jet fragmentation*, Z. Phys. **C20** (1983), 317.

[270] B. Andersson and G. Gustafson, *Semiclassical Models for Gluon Jets and Leptoproduction Based on the Massless Relativistic String*, Z. Phys. C **3** (1980), 223.

[271] T. Sjöstrand, *Jet Fragmentation of Nearby Partons*, Nucl.Phys. **B248** (1984), 469.

[272] B. Andersson, G. Gustafson and T. Sjöstrand, *A Model for Baryon Production in Quark and Gluon Jets*, Nucl. Phys. **B197** (1982), 45.

[273] T. Sjöstrand, *The Lund Monte Carlo for Jet Fragmentation*, Comput. Phys. Commun. **27** (1982), 243.

[274] B. Andersson, *The Lund Model*, Cambridge Monographs on Particle Physics, Nuclear Physics and Cosmology, vol. 7, Cambridge University Press, 7 2023.

[275] T. Sjöstrand, S. Mrenna and P. Skands, *PYTHIA 6.4 physics and manual*, JHEP **05** (2006), 026, [hep-ph/0603175].

[276] F. Siegert, *Simulation of hadron decays in SHERPA*, Diploma thesis.

[277] T. Laubrich, *Implementation of tau-lepton decays into the event generator Sherpa*, Diploma Thesis.

[278] S. Jadach, Z. Was, R. Decker and J. H. Kühn, *The tau decay library TAUOLA: Version 2.4*, Comput. Phys. Commun. **76** (1993), 361–380.

[279] D. J. Lange, *The EvtGen particle decay simulation package*, Nucl. Instrum. Meth. **A462** (2001), 152–155.

[280] W. T. Giele, D. A. Kosower and P. Z. Skands, *Higher-Order Corrections to Timelike Jets*, Phys. Rev. **D84** (2011), 054003, [arXiv:1102.2126 [hep-ph]].

[281] S. Mrenna and P. Skands, *Automated Parton-Shower Variations in Pythia 8*, Phys. Rev. **D94** (2016), no. 7, 074005, [arXiv:1605.08352 [hep-ph]].

[282] J. Bellm, S. Plätzer, P. Richardson, A. Siódmok and S. Webster, *Reweighting Parton Showers*, Phys. Rev. **D94** (2016), no. 3, 034028, [arXiv:1605.08256 [hep-ph]].

[283] C. Bierlich, P. Ilten, T. Menzo, S. Mrenna, M. Szewc, M. K. Wilkinson, A. Youssef and J. Zupan, *Reweighting Monte Carlo predictions and automated fragmentation variations in Pythia 8*, SciPost Phys. **16** (2024), no. 5, 134, [arXiv:2308.13459 [hep-ph]].

[284] E. Bothmann, M. Schönherr and S. Schumann, *Reweighting QCD matrix-element and parton-shower calculations*, Eur. Phys. J. **C76** (2016), no. 11, 590, [arXiv:1606.08753 [hep-ph]].

[285] M. Dobbs and J. B. Hansen, *The HepMC C++ Monte Carlo event record for High Energy Physics*, Comput. Phys. Commun. **134** (2001), 41–46.

[286] A. Buckley, P. Ilten, D. Konstantinov, L. Lönnblad, J. Monk, W. Pokorski, T. Przedzinski and A. Verbytskyi, *The HepMC3 event record library for Monte Carlo event generators*, Comput. Phys. Commun. **260** (2021), 107310, [arXiv:1912.08005 [hep-ph]].

[287] C. Bierlich et al., *Robust Independent Validation of Experiment and Theory: Rivet version 3*, SciPost Phys. **8** (2020), 026, [arXiv:1912.05451 [hep-ph]].

[288] C. Bierlich, A. Buckley, J. Butterworth, C. Gutschow, L. Lonnblad, T. Procter, P. Richardson and Y. Yeh, *Robust Independent Validation of Experiment and Theory: Rivet version 4 release note*, arXiv:2404.15984 [hep-ph].

[289] A. Buckley, J. Butterworth, L. Lönnblad, D. Grellscheid, H. Hoeth et al., *Rivet user manual*, Comput.Phys.Commun. **184** (2013), 2803–2819, [arXiv:1003.0694 [hep-ph]].

[290] L. Del Debbio, N. P. Hartland and S. Schumann, *MCgrid: projecting cross section calculations on grids*, Comput. Phys. Commun. **185** (2014), 2115–2126, [arXiv:1312.4460 [hep-ph]].

[291] E. Bothmann, N. Hartland and S. Schumann, *Introducing MCgrid 2.0: Projecting cross section calculations on grids*, Comput. Phys. Commun. **196** (2015), 617–618.

[292] T. Carli et al., *A posteriori inclusion of parton density functions in NLO QCD final-state calculations at hadron colliders: The APPLGRID Project*, Eur. Phys. J. **C** (2010), 503–524, [arXiv:0911.2985 [hep-ph]].

[293] D. Britzger, K. Rabbertz, F. Stober and M. Wobisch, *New features in version 2 of the fastNLO project*, Proceedings, 20th International Workshop on Deep-Inelastic Scattering and Related Subjects (DIS 2012): Bonn, Germany, March 26-30, 2012, 2012, pp. 217–221.

[294] A. Banfi, G. P. Salam and G. Zanderighi, *Generalized resummation of QCD final state observables*, Phys.Lett. **B584** (2004), 298–305, [arXiv:hep-ph/0304148 [hep-ph]].

[295] A. Banfi, G. P. Salam and G. Zanderighi, *Principles of general final-state resummation and automated implementation*, JHEP **03** (2005), 073, [arXiv:hep-ph/0407286 [hep-ph]].

[296] E. Gerwick, S. Höche, S. Marzani and S. Schumann, *Soft evolution of multi-jet final states*, JHEP **02** (2015), 106, [arXiv:1411.7325 [hep-ph]].

[297] S. Marzani, D. Reichelt, S. Schumann, G. Soyez and V. Theeuwes, *Fitting the Strong Coupling Constant with Soft-Drop Thrust*, JHEP **11** (2019), 179, [arXiv:1906.10504 [hep-ph]].

[298] D. Reichelt, S. Caletti, O. Fedkevych, S. Marzani, S. Schumann and G. Soyez, *Phenomenology of jet angularities at the LHC*, JHEP **03** (2022), 131, [arXiv:2112.09545 [hep-ph]].

[299] Y.-T. Chien, O. Fedkevych, D. Reichelt and S. Schumann, *Jet angularities in dijet production in proton-proton and heavy-ion collisions at RHIC*, JHEP **07** (2024), 230, [arXiv:2404.04168 [hep-ph]].

[300] D. d'Enterria et al., *The strong coupling constant: State of the art and the decade ahead*, arXiv:2203.08271 [hep-ph].

[301] S. Caletti, O. Fedkevych, S. Marzani, D. Reichelt, S. Schumann, G. Soyez and V. Theeuwes, *Jet angularities in Z+jet production at the LHC*, JHEP **07** (2021), 076, [arXiv:2104.06920 [hep-ph]].

[302] S. Caletti, O. Fedkevych, S. Marzani and D. Reichelt, *Tagging the initial-state gluon*, Eur. Phys. J. C **81** (2021), no. 9, 844, [arXiv:2108.10024 [hep-ph]].

[303] V. Andreev et al., H1 collaboration, *Measurement of the 1-jettiness event shape observable in deep-inelastic electron-proton scattering at HERA*, Eur. Phys. J. C **84** (2024), no. 8, 785, [arXiv:2403.10109 [hep-ex]].

[304] V. Andreev et al., H1 collaboration, *Measurement of groomed event shape observables in deep-inelastic electron-proton scattering at HERA*, Eur. Phys. J. C **84** (2024), no. 7, 718, [arXiv:2403.10134 [hep-ex]].

[305] M. Knobbe, D. Reichelt, S. Schumann and L. Stöcker, *Precision calculations for groomed event shapes at HERA*, arXiv:2407.02456 [hep-ph].

[306] A. Gehrmann-De Ridder, C. T. Preuss, D. Reichelt and S. Schumann, *NLO+NLL' accurate predictions for three-jet event shapes in hadronic Higgs decays*, JHEP **07** (2024), 160, [arXiv:2403.06929 [hep-ph]].

[307] C. W. Bauer, S. Fleming, D. Pirjol and I. W. Stewart, *An Effective field theory for collinear and soft gluons: Heavy to light decays*, Phys.Rev. **D63** (2001), 114020, [arXiv:hep-ph/0011336 [hep-ph]].

[308] C. W. Bauer, D. Pirjol and I. W. Stewart, *Soft collinear factorization in effective field theory*, Phys.Rev. **D65** (2002), 054022, [arXiv:hep-ph/0109045 [hep-ph]].

[309] W.-L. Ju and M. Schönherr, *The q_T and $\Delta\phi$ spectra in W and Z production at the LHC at $N^3LL'+N^2LO$*, JHEP **10** (2021), 088, [arXiv:2106.11260 [hep-ph]].

[310] W.-L. Ju and M. Schönherr, *Projected transverse momentum resummation in top-antitop pair production at LHC*, JHEP **02** (2023), 075, [arXiv:2210.09272 [hep-ph]].

[311] W.-L. Ju and M. Schönherr, *The q_{T} and $\Delta\phi_{t\bar{t}}$ spectra in top-antitop hadroproduction at NNLL+NNLO: the interplay of soft-collinear resummation and Coulomb singularities*, arXiv:2407.03501 [hep-ph].

[312] G. Ferrera, W.-L. Ju and M. Schönherr, *Zero-bin subtraction and the q_T spectrum beyond leading power*, JHEP **04** (2024), 005, [arXiv:2312.14911 [hep-ph]].

[313] S. Amoroso et al., HSF Physics Event Generator WG collaboration, *Challenges in Monte Carlo Event Generator Software for High-Luminosity LHC*, Comput. Softw. Big Sci. **5** (2021), no. 1, 12, [arXiv:2004.13687 [hep-ph]].

[314] S. Amoroso et al., HSF Physics Event Generator WG collaboration, *Challenges in Monte Carlo event generator software for High-Luminosity LHC*, arXiv:2004.13687 [hep-ph].

[315] E. Yazgan et al., HSF Physics Event Generator WG collaboration, *HL-LHC Computing Review Stage-2, Common Software Projects: Event Generators*, arXiv:2109.14938 [hep-ph].

[316] G. Aad et al., ATLAS collaboration, *Modelling and computational improvements to the simulation of single vector-boson plus jet processes for the ATLAS experiment*, JHEP **08** (2022), 089, [arXiv:2112.09588 [hep-ex]].

[317] E. Bothmann, W. Giele, S. Höche, J. Isaacson and M. Knobbe, *Many-gluon tree amplitudes on modern GPUs: A case study for novel event generators*, SciPost Phys. Codeb. **2022** (2022), 3, [arXiv:2106.06507 [hep-ph]].

[318] E. Bothmann, J. Isaacson, M. Knobbe, S. Höche and W. Giele, *QCD tree amplitudes on modern GPUs: A case study for novel event generators*, PoS **ICHEP2022** (2022), 222.

[319] E. Bothmann, T. Childers, W. Giele, F. Herren, S. Höche, J. Isaacson, M. Knobbe and R. Wang, *Efficient phase-space generation for hadron collider event simulation*, SciPost Phys. **15** (2023), no. 4, 169, [arXiv:2302.10449 [hep-ph]].

[320] E. Bothmann, T. Childers, W. Giele, S. Höche, J. Isaacson and M. Knobbe, *A Portable Parton-Level Event Generator for the High-Luminosity LHC*, SciPost Phys. **17** (2024), 081, [arXiv:2311.06198 [hep-ph]].

[321] A. Buckley, L. Corpe, M. Filipovich, C. Gutschow, N. Rozinsky, S. Thor, Y. Yeh and J. Yellen, *Consistent, multidimensional differential histogramming and summary statistics with YODA 2*, arXiv:2312.15070 [hep-ph].

[322] E. Bothmann, T. Janßen, M. Knobbe, T. Schmale and S. Schumann, *Exploring phase space with Neural Importance Sampling*, SciPost Phys. **8** (2020), no. 4, 069, [arXiv:2001.05478 [hep-ph]].

[323] C. Gao, S. Höche, J. Isaacson, C. Krause and H. Schulz, *Event Generation with Normalizing Flows*, Phys. Rev. D **101** (2020), no. 7, 076002, [arXiv:2001.10028 [hep-ph]].

[324] G. P. Lepage, *VEGAS - An Adaptive Multi-dimensional Integration Program*, CLNS-80/447.

[325] K. Danziger, T. Janßen, S. Schumann and F. Siegert, *Accelerating Monte Carlo event generation – rejection sampling using neural network event-weight estimates*, SciPost Phys. **12** (2022), 164, [arXiv:2109.11964 [hep-ph]].

[326] D. Maître and H. Truong, *A factorisation-aware Matrix element emulator*, JHEP **11** (2021), 066, [arXiv:2107.06625 [hep-ph]].

[327] T. Janßen, D. Maître, S. Schumann, F. Siegert and H. Truong, *Unweighting multijet event generation using factorisation-aware neural networks*, SciPost Phys. **15** (2023), no. 3, 107, [arXiv:2301.13562 [hep-ph]].

[328] B. Abi et al., DUNE collaboration, *Prospects for beyond the Standard Model physics searches at the Deep Underground Neutrino Experiment*, Eur. Phys. J. C **81** (2021), no. 4, 322, [arXiv:2008.12769 [hep-ex]].

[329] B. Abi et al., DUNE collaboration, *Deep Underground Neutrino Experiment (DUNE), Far Detector Technical Design Report, Volume II: DUNE Physics*, arXiv:2002.03005 [hep-ex].

[330] K. Abe et al., Hyper-Kamiokande collaboration, *Hyper-Kamiokande Design Report*, arXiv:1805.04163 [physics.ins-det].

[331] R. Acciarri et al., MicroBooNE, LAr1-ND, ICARUS-WA104 collaboration, *A Proposal for a Three Detector Short-Baseline Neutrino Oscillation Program in the Fermilab Booster Neutrino Beam*, arXiv:1503.01520 [physics.ins-det].

[332] J. Isaacson, S. Höche, D. Lopez Gutierrez and N. Rocco, *Novel event generator for the automated simulation of neutrino scattering*, Phys. Rev. D **105** (2022), no. 9, 096006, [arXiv:2110.15319 [hep-ph]].

[333] E. Hernández, J. Nieves, F. Sánchez and J. E. Sobczyk, *Tau longitudinal and transverse polarizations from visible kinematics in (anti-)neutrino nucleus scattering*, Phys. Lett. B **829** (2022), 137046, [arXiv:2202.07539 [hep-ph]].

[334] J. Isaacson, S. Höche, F. Siegert and S. Wang, *Tau polarization and correlated decays in neutrino experiments*, Phys. Rev. D **108** (2023), no. 9, 093004, [arXiv:2303.08104 [hep-ph]].

[335] L. Alvarez-Ruso et al., GENIE collaboration, *Recent highlights from GENIE v3*, Eur. Phys. J. ST **230** (2021), no. 24, 4449–4467, [arXiv:2106.09381 [hep-ph]].

[336] C. Andreopoulos et al., *The GENIE Neutrino Monte Carlo Generator*, Nucl. Instrum. Meth. A **614** (2010), 87–104, [arXiv:0905.2517 [hep-ph]].

[337] O. Buss, T. Gaitanos, K. Gallmeister, H. van Hees, M. Kaskulov, O. Lalakulich, A. B. Larionov, T. Leitner, J. Weil and U. Mosel, *Transport-theoretical Description of Nuclear Reactions*, Phys. Rept. **512** (2012), 1–124, [arXiv:1106.1344 [hep-ph]].

[338] Y. Hayato and L. Pickering, *The NEUT neutrino interaction simulation program library*, Eur. Phys. J. ST **230** (2021), no. 24, 4469–4481, [arXiv:2106.15809 [hep-ph]].

[339] Y. Hayato, *A neutrino interaction simulation program library NEUT*, Acta Phys. Polon. B **40** (2009), 2477–2489.

[340] T. Golan, J. T. Sobczyk and J. Zmuda, *NuWro: the Wroclaw Monte Carlo Generator of Neutrino Interactions*, Nucl. Phys. B Proc. Suppl. **229-232** (2012), 499–499.

[341] O. Ben-Kiki, C. Evans and B. Ingerson, *YAML Ain't Markup Language (YAML) (tm) Version 1.2*, Tech. report, YAML.org, 10 2009.